15. ANIMALS AND THE ATMOSPHERE: LARGE ANIMALS INCLUDING MAN

Introduction

In this Chapter we will consider several matters — mainly physiological — that are distinctly more important in the lives of large animals than in the lives of small animals. The materials we present to illustrate these matters are taken from studies of both Man and other large animals, but we make no general claim that the results apply equally well in all cases to both groups. Just the same, what we present will help make clear the ways in which large animals differ most importantly from small animals, biometeorologically speaking.

All thermostatic controls require energy for construction, maintenance, and operation. Because larger animals have a smaller weight-specific requirement for metabolic energy simply to support basal metabolism, they have more energy available for more complex methods of heat energy control — for "fine tuning" their thermoregulation. Whereas small animals specialize in the use of a basic set of controls consisting mainly of movement and variable metabolic rate, large animals make use of the full range of energy controls considered in **Chapter 13**.

As we have remarked earlier that the role of metabolic energy in the heat economy of animals is enormously more important than in plants, and it often represents the largest component by far in the energy balance of an animal. As we have also indicated earlier, the metabolic rates of humans and other large animals, compared with small animals, are much less variable under conditions of a widely varying thermal environment. Although the metabolic rate of large animals changes markedly as their level of physical activity — work and sport — varys, their basal rates are, for all practical purposes, constant. The complexity of the system of controls producing this result is impressive. In this Chapter we will provide some basic physiological insight into this complexity.

In the mathematical modeling of the animal energy balance developed in this chapter, we extend our earlier presentations by emphasizing four kinds of thermoregulatory control. First is the shape, posture, and orientation of the body as they affect the shortwave radiant heat load and the convective dissipation of sensible heat by the wind. Second, we give particular attention to the variable body resistance to heat flow. Third, we consider the role of the coat in controlling the

flow of heat between the body and the environment; and, finally, we examine the response of evaporative cooling to changes in the atmospheric environment.

In **Chapters 16** and **17** we extend still farther our treatment of the energy balance of Man by giving particular attention to the two controls that distinguish Man from other large animals: removable clothing and architecture. These two types of control illustrate most vividly the comment made earlier regarding the energy required for construction, maintenance, and operation of thermoregulatory controls. Before we consider these physiological matters of difference in this Chapter, however, we first discuss one of the ways in which all animals may be regarded as similar: the preferendum.

Atmospheric effects on the Preferendum of large animals

In **Chapter 14** we remarked that the concept of the preferendum, based on fully- or partly-controlled experiments, may seem somewhat artificial in the sense that only those environments can be "preferred" that have been made available to the animals. Countering this notion of artificiality, however, is the fact that the natural world more often than not consists of discrete "patches" of available environments rather than a set of gradients. In order not to leave the reader with the impression that the concept of the preferendum applies only to small animals, we present a brief examination of the concept at work in an elk herd in Yellowstone Park and in some human beings.

As indicated earlier, we suggest that the effects of abundance and scarcity of food may be thought of as the "footprints" left by earlier weather events on the environments and, though them, on the lives of today's animal populations. For the elk (*Cervus elaphus*) in mountainous Yellowstone Park the locations and abundance of food made available by the growing season of the previous summer, the locations and conditions of their predators, and the ambient depth and condition of snow during winter, all combine to present the overwintering elk with a patchwork of field environments from which to choose. The patch boundaries are determined primarily by elevation, and secondarily by slope and aspect(A). As an atmospheric effect in addition to that on the abundance and scarcity of food, greater low-temperature thermal stress on the animals decreases their fat reserves and, thus, their ability to tolerate adversity. This, in turn, affects the herd mortality; and, for the survivors, their choices of location as winter progresses(I).

The elk herd migrates to higher elevations in late spring, following the development of new vegetation. It spends the summer feeding at the highest elevations in the region, which are snow-free and which

(A) The aspect of a site is the direction in which it faces.

present the most luxuriant mid-summer forage regionally available. The elevation of the lower boundary of the area occupied by the herd in summer tends to be inversely related to the size of the herd. That is, for example, in a summer when herd numbers are larger than normal, depending in part on conditions over the previous year, the lowest animals are found at elevations that are lower than normal because the herd tends to maintain an upper limit on is own spatial density. Thus, in any year the summer feeding takes place in topographically determined spatial "patches", disjunct from one another.

A dry summer severely curtails forage production everywhere in the Park, sending the herd into winter with only a limited fat reserve. In this condition the animals, during the following winter, are less able than following a normal summer to tolerate in winter the physical drain on their limited energy supply caused by deep snow. Although it inhibits predators, deep snow also increases the costs to the elk of searching and digging for food. Different combinations of these various factors, from year to year, determine both the date in winter when the herd begins to migrate to lower elevations and the condition of the animals when they arrive.

Fig. 15-1, based on many decades of animal counts and snow measurements, sketches the generalized relationship between the snowpack water equivalent (SWE) and the elevations at which the herd is found at various times throughout the winter. At a constant elevation, reading from left to right in this generalized presentation, the snowpack becomes deeper between late October and late March. The elk herd is distributed vertically across an elevational band whose width remains relatively constant through January, at which time the snowpack reaches the maximum depth and density the animals can tolerate. At this time the median elevation of the herd is near the contour of 12cm for the SWE. As snow continues to accumulate, the herd

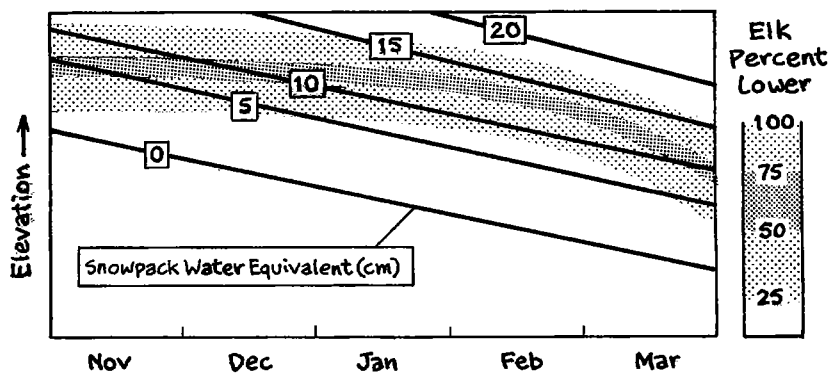

Fig. 15-1 In a typical year, the elk herd in Yellowstone National Park moves, in response to a set of factors, to different elevations between early winter and early spring. The figure is a generalized presentation of those movements as they are related to one of the factors: the snow pack[1].

moves to lower elevations, following the 12cm SWE contour, which corresponds to the limit of their tolerance. As their physical stamina is drained in early March, the animals must move still lower to a less limiting, slightly shallower snowpack of about 10cm SWE.

In principle, members of the elk herd are free to choose locations anywhere in the full range of elevations shown in the figure. However, they make the choices indicated, thereby seeking their "preferendum." The factors shaping that preferendum, in addition to snow depth, are those discussed at some length in **Chapter 14**: crowding, availability of food, location of predators, and temperature.

We close this section with a comment on the idea that human beings, too, may seek a preferendum. From one point of view we may say that the preferenda of animals are based on energetics — the management of metabolic and environmental heat energy — whereas the preferenda of people are based on comfort — the movement to locations in which we feel comfortable. From that point of view, one's comfort is separable from one's heat energy balance. *Comfort* is a human concept applicable only to ourselves. Animals don't feel, or not feel, comfortable.

From the opposing point of view, "comfort" is the term human beings use for their feeling of being in a condition of thermoneutrality, in which they do not need to expend energy in the use of thermoregulatory controls to achieve thermal equilibrium. Comfort is thus the absence of thermal stress.

Human beings typically move to locations, from among the locations available, that most nearly result in effortless thermoneutrality. From that point of view, animals are doing the same when they seek a preferendum, although we don't apply the word "comfort" to them. We may be said to express our preferendum when we cross to the sunny side of the street on a cold day or choose to sit in the shade on a hot day. Likewise, human beings may be expressing their preferendum when they spend all or part of their winters in a warmer climate or their summers in a cool area. Examination of the personal heat energy balance of such people leaves little doubt that they are doing exactly what animals do: seeking long-term thermoneutrality without having to resort to the expenditure of energy in thermoregulatory controls.

The matter, however, is not quite so simply set aside. A large fraction of the research effort in the earliest times of modern biometeorology consisted of studies — especially by European scientists — of the relationships between certain medical conditions and the atmospheric circumstances that caused them to be more or less incapacitating. These conditions were mainly respiratory, associated with living in an urban, industrial environment[2]. The atmospheric variables involved in the studies were mainly barometric pressure and its rates of change, air quality as related to air ions and aerosols, and the ultraviolet component of solar radiation.

The focus of what was a "culture of medical bioclimatology" was centered on finding and publicizing localities that offered the medically most beneficial combination of high altitude and dry, cloud-free days. They were found mainly in the mountains of southern Europe, where the high altitudes at those latitudes produce a combination of greater and more reliable fluxes of ultraviolet with relatively unvarying pressure. The commercial aspects of these preferenda became intertwined with the experimental scientific aspects; and a sub-culture of *resort climatology* flourished just before World War II, which persists even today in many countries. The most successful resorts, of course, were able, in a highly competitive market, to advertise their local mineral waters, which, combined with the local climate, led to claims of "cures" for particular ailments.

Out of the commercialism of this movement there also came a funding for genuine research in the physiological and medical aspects of human biometeorology. Later, much of this financial support was taken over by programs in military medicine, which developed when it became evident that, in the modern world, a single individual in uniform might have to operate in any of several extremes of atmospheric adversity in many climatic regions. Today's *space medicine* is the farthest point of development in this field. We mention these aspects of biometeorology merely to make the point that human beings — especially wealthy ones — seek atmospheric preferenda for reasons not simply expressed in terms of their heat energy balance and thermoneutrality. With this brief consideration of the concept of human comfort we have introduced a subject that will occupy much of our discussion later in **Chapters 16** and **17**.

The metabolic work rate and body temperature in Man

Recalling our earlier comment about the response of the metabolic rate of a large animal to heightened physical activity, we present **Table 15-1**, which provides a representative list of equivalents, expressed in two units: (Wm^{-2}) from the SI system, and (Mets) from the system customarily long used in the literature on human medical and physiological biometeorology. The basal metabolic rate for an adult human being is taken as the definition of 1 Met.

The physical activity represented by the entries in **Table 15-1** generates metabolic heat at a rate in excess of the basal rate, thereby altering the body's energy balance. There is no single "body temperature" — a temperature that is equally representative of all parts of the thermoregulating body — that responds to the changing metabolic rate. To begin our considerations of the relationships among environmental temperature, several body temperatures, and the work rate we present two data sets in **Table 15-2**.

First, we can connect the information in **Tables 15-1** and **15-2**. For example, note that the metabolic rates in **Table 15-1** are expressed in (Wm^{-2}), whereas in **Table 15-2**, Set A, they are expressed in (Wkg^{-1}).

TABLE 15-1 REPRESENTATIVE METABOLIC ENERGY EQUIVALENTS TO ORDINARY ACTIVITIES OF MAN

Human activity	Equivalent in (Mets)	Equivalent in (W m^{-2}) (Mean of Met values)
Supine rest, sitting, standing, eating	1	57.9
Dressing, washing, driving	2	115.8
Light housework	2 - 3.5	159.2
Golf with power cart, bowling	2 - 4	173.7
Walking at 2.5 km/hr	3	173.7
Showering	3.5	202.7
Walking downstairs	4.5	260.6
Walking at 3.5 km/hr	5.5	318.5
Cycling, conditioning exercise	3 - 8	318.5
Golf walking, dancing	4 - 8	347.4
Swimming	5 - 8	376.4
Climbing stairs, 1 flight, tennis	6 - 9	434.3
Walking uphill	5.5 - 10	448.7
Jogging at 5 km/hr	9	521.1
Handball, raquetball	8 - 12	579.0
Jumping rope	9 - 12	608.0
Jogging at 10 km/hr	16	926.4

SOURCE: DuPont and Freedman (1983), page 261.
NOTES:
(a) 1 Met = 50 kcal m^{-2} hr^{-1} = 57.87 W m^{-2}.
(b) To a first approximation for walking and jogging: Met = 1 + 1.5(km/hr)

By using the representative values of 86kg and 1.9m^2 for a typical adult human being, we can compare the metabolic rates between the two tables. After conversion, the smallest and the largest rates in **Table 15-2**, Set A, are 60.7 and 667 (Wm^{-2}), equivalent approximately to 1 and 11.5 Mets. The entries in both **Tables 15-1** and **15-2**, Set A, then, represent the full range of activity from resting to vigorous exercise.

To illustrate our earlier remark that there is no single body temperature that responds to the changing metabolic rate, we present **Fig. 15-2**, based on the data in **Table 15-2**, Set A. The metabolic rate is related to the rectal temperature, ($\mathbf{T_{re}}$), in **Fig. 15-2a** and to the skin temperature, ($\mathbf{T_{sk}}$), in **Fig. 15-2b**. Both panels include information on the operative temperature(B), ($\mathbf{T_{op}}$), and together they demonstrate several points:

(a) ($\mathbf{T_{sk}}$) — ranging between about 27 and 35 °C — is much more variable than is ($\mathbf{T_{re}}$), which ranges only between 37 and 38.6 °C (note the different temperature scales in the two panels);
(b) ($\mathbf{T_{re}}$) is highly correlated with the metabolic rate, (**M**), but not with ($\mathbf{T_{op}}$); whereas
(c) ($\mathbf{T_{sk}}$) is highly correlated with ($\mathbf{T_{op}}$) but not with (**M**).

(B) Concerning the operative temperature, ($\mathbf{T_{op}}$), see **Eq.(14-3a)** and **Note (26)** of **Chapter 14**.

TABLE 15-2 OBSERVATIONAL DATA CONNECTING TEMPERATURES, RATE OF WORK, AND RATE OF SWEATING IN MAN

Observation Number	Operative temperature $T_{(op)}$(°C)	Skin temperature $T_{(sk)}$(°C)	Rectal temperature $T_{(re)}$(°C)	Core[a] temperature $T_{(c)}$(°C)	Metabolic rate (W/kg)[b]	Rate of sweating (W/m²)[c]
Data set A						
1	10.5	29.4	37.9	37.05[a]	7.04	34.
2	10.5	29.4	37.95	37.16	7.04	68.
3	10.5	29.4	38.0	36.98	7.04	13.6
4	10.5	27.3	38.3	37.37	11.73	129.2
5	10.5	28.9	38.6	37.85	14.74	272.
6	10.5	28.1	36.8	36.98	1.68	13.6
7	25.2	34.4	37.1	37.05	1.34	34.
8	25.2	34.1	37.6	37.30	5.03	108.8
9	25.2	33.7	38.0	37.65	9.38	210.8
10	25.2	34.0	38.2	37.99	11.73	312.8

SOURCE OF SET A: Ingram and Mount (1975), Figure 10-2, based on data due to Robinson.
NOTES:
(a) The core temperature was estimated from the relationship in Data Set B: $T_c = 36.96 + 0.0034$ (SR), where (SR) is the sweat rate in (W/m²).
(b) The units for metabolic rate in the source are a physiological measure of the rate of work: the rate of oxygen intake, which is 1 ml O_2 min^{-1} = 0.335 W.
(c) The units for sweating rate in the source are $cm^3m^{-2}hr^{-1}$. Our conversion to (W/m²) is based on the assumption of the evaporation of all sweat, a reasonable assumption for the physiological laboratory environment.

Observation Number	Operative[d] temperature $T_{(op)}$(°C)	Skin temperature $T_{(sk)}$(°C)	Rectal[e] temperature $T_{(re)}$(°C)	Core[a] temperature $T_{(c)}$(°C)	Metabolic rate (W/kg)[f]	Rate of sweating (W/m²)[g]
Data set B						
11	31.1[d]	36.5	37.32[e]	37.38	3.85[f]	127.2
12	31.1	36.5	37.31	37.31	3.67	120.6
13	31.6	36.7	37.38	37.35	3.49	120.6
14	30.0	36.1	37.21	37.22	2.90	78.9
15	30.3	36.2	37.18	37.17	2.63	72.4
16	29.0	35.7	37.13	37.04	2.20	39.5
17	26.6	34.8	37.13	36.94	2.25	11.
18	28.2	35.4	37.50	37.38	5.27	142.5
19	26.6	34.8	37.40	37.27	4.45	92.1
20	23.8	33.7	37.44	37.14	4.81	68.
21	29.3	35.8	37.51	37.45	5.33	157.9
22	26.6	34.8	37.49	37.35	5.23	120.6
23	23.2	33.5	37.55	37.25	5.65	92.1
24	22.5	33.2	37.41	37.09	4.49	39.5

SOURCE OF SET B: T.H. Benzinger, SCIENTIFIC AMERICAN, January 1961, page 233.
NOTES:
(d) The operative temperature was estimated from the relationship in Data Set A: $T_{op} = 2.616\ (T_{skin}) - 64.4$.
(e) The rectal temperature was estimated from the relationship in Data Set A: $T_{re} = 40.97 - 0.1113\ (T_{skin}) + 0.0033$ (SR) with $r^2 = 0.9993$.
(f) The units for metabolic rate in the source are calories sec^{-1} above resting. We have substituted an estimate from the relationship in Data Set A: $M = (T_{re} - 36.86)/0.1214$ with $r^2 = 0.96$.
(g) The units for sweat rate in the source are calories sec^{-1}. We have assumed an area of 1.9 m².

In fact, the text in the source for **Table 15-2**, Set A, includes the statement that "The increments in rectal temperature were produced by increasing intensities of work."

In addition to the operative temperature, (T_{op}), skin temperature, (T_{sk}), and rectal temperature, (T_{re}), we need to consider the body's core temperature, (T_c), in order to complete our discussion of the effects of the environment and the variable metabolic work rate on the body's thermoregulatory system. The body's core temperature is best thought of as that of the blood flow in the main arteries entering the brain, which is essentially the same as the temperature in the nearby core of the body. In fact, as we will see later when considering the use of evaporative cooling, the thermoregulatory system

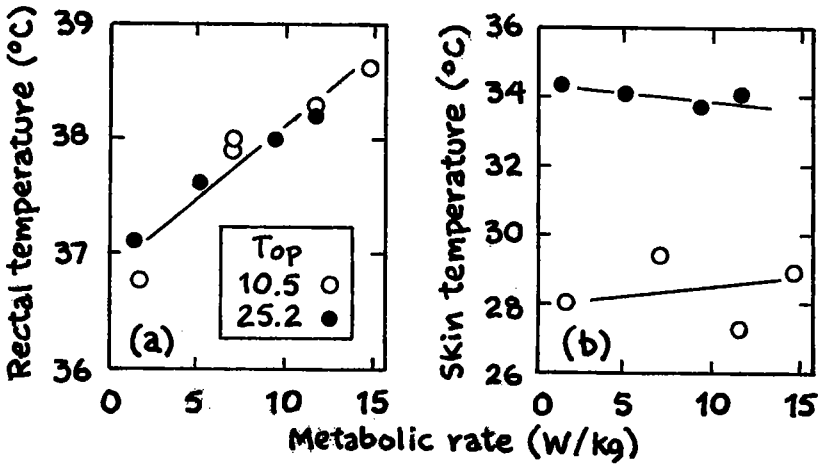

Fig. 15-2 The data in **Table 15-2**, Set A, demonstrate the facts that **(a)** the observed human rectal temperature, (T_{re}), is highly correlated with the observed metabolic rate, (**M**); whereas **(b)** the skin temperature, (T_{sk}), is highly correlated with the the operative temperature, (T_{op}), and not with (**M**).

senses that blood temperature near the base of the brain. Any difference between that (T_c) and the *set point* of a healthy body — always near 36.9 °C — acts as an *error signal*. The system is "triggered" when the error signal departs from zero. A negative error signal activates the negative feedback of shivering, and a positive error signal activates the negative feedback of increased body conductivity and sweating at rates proportional to the size of the error signal.

Fig. 15-3 presents a generalized sketch of relationships among these four temperatures. More specifically, the figure shows the range of values, for each, found in **Table 15-2**. We can note two additional features:

(d) (T_{op}) is much more variable than is (T_{sk}); and
(e) as one proceeds inward from the atmospheric environment to the body's core, the temperatures become both warmer and less variable.

Fig. 15-3 depicts the normal state of affairs: the general temperature gradient from a warm core to a less warm environment indicates that the body loses heat to the environment whenever the thermoregulatory system operates successfully. The decreasing variability of

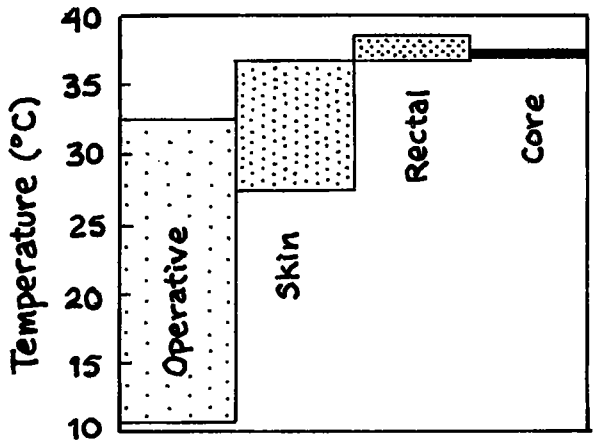

Fig. 15-3 The ranges of values of four temperatures in both data sets of **Table 15-2** show the generalized relationships among them. See the text for discussion.

temperatures as one proceeds inward is consistent with the fact that the center of the thermoregulatory system lies well within the body.

We have considered in the last two chapters how ($\mathbf{T_{op}}$) is a weighted mean of various environmental temperatures. Similarly, the skin temperature, ($\mathbf{T_{sk}}$), is a weighted mean of temperatures over several areas of the air-skin interface. Exactly which areas are involved in the calculation of the mean, of course, depends upon the experimental arrangements involved in any particular study. We do not know those arrangements in either of the experiments represented in **Table 15-2**, but we have already seen that ($\mathbf{T_{sk}}$) is controlled largely by, but is less variable than ($\mathbf{T_{op}}$). While the skin temperature reported by an experimenter is a weighted mean of temperatures over several areas, ($\mathbf{T_{re}}$) is essentially a point-specific value that depends mainly on the metabolic work rate, (**M**), and is essentially independent of conditions outside the body, as represented by ($\mathbf{T_{op}}$) and ($\mathbf{T_{sk}}$). We have already noted how ($\mathbf{T_c}$) — also a point-specific value — is involved directly in the negative feeedback of a system that senses (T_c - 36.9) as an error signal.

Fig. 15-4 presents two additional, generalized sketches of relationships among the four temperatures we are considering. Based on **Table 15-2**, Set A, **Fig. 15-4a** makes the point that the sizes of temperature *differences* in the system respond mostly to changes in ($\mathbf{T_{op}}$), with much less response to changes in (**M**), which is represented by the error bars in **Fig. 15-4a**.

Fig. 15-4b summarizes, in the form of temperature profiles, the relationships among the four temperatures and the metabolic work rate for the two conditions of resting and working. This sketch reinforces earlier conclusions regarding temperature differences, but it includes the additional information, not exhibited graphically before now, that

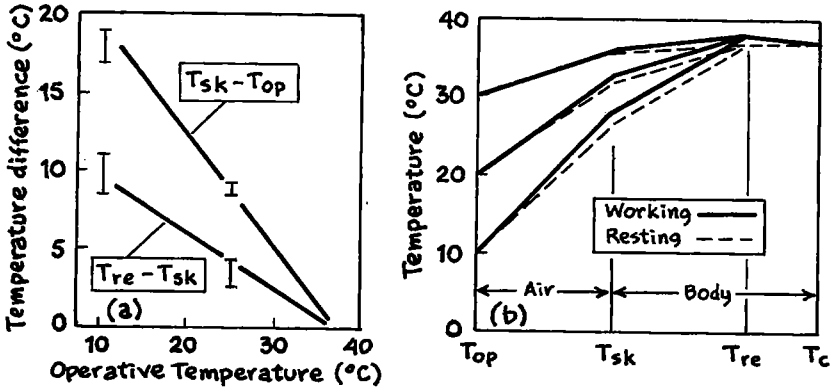

Fig. 15-4 Two generalized sketches relate temperatures and temperature differences associated with the human body. **(a)** The lines show predictable relationships between (T_{op}) and two temperature differences: the rectal-skin and the skin-environment. The error bars indicate the range of variation in an observed temperature difference associated with the range of the metabolic work rate in the data of **Table 15-2**, Set A. **(b)** The same relationships are presented in the form of temperature profiles. See the text for discussion.

(f) (T_{re}) may rise above (T_c); and
(g) (T_c) does not, for all practical purposes, respond to (**M**).

Finally, we remark that (T_{re}) and (T_c) have essentially the same value under conditions of a thermal steady state and in slowly changing conditions. However, (T_c) is best viewed as the temperature of a small mass with a small thermal time constant; whereas, (T_{re}) can be viewed as the temperature of a large mass with a larger thermal time constant[C]. For example, (T_c) responds rapidly to the ingestion of hot or cold foods and liquids, but (T_{re}) does not. Such short-term effects on (T_c) will disappear quickly, however; and the two temperatures will again be the same.

The variable thermal conductivity of body and coat in a large animal

Large animals, in contrast with small ones, make use of a variable cardiovascular system and evaporative cooling, rather than a variable metabolic rate, for fine-tuning their energy balance. We have noted how these two responses are "triggered" by a thermal error signal; whereas, coarse tuning is accomplished mostly by changes in location, clothing or coat, and posture. We examine the system of evaporative cooling in the next section. First — in this section, and in **Box 15-1** — we consider the variable cardiovascular system and the use of hair- and feather-coats.

(C) Regarding the thermal time constant, refer to **Box 13-2**.

In its simplest form, we have generally represented the flow of heat in a conducting pathway, such as any one of those in **Fig. 15-4b**, by a flow-gradient relationship. For example, the flow between the body core and the skin would be

$$\text{Heat flow} = k_b\,(dT/dz) = k_b\,(T_c - T_{sk})/(d_b) \qquad (15\text{-}1a)$$

in which the thermal conductivity of the body mass is ($\mathbf{k_b}$) and its conductance is $h_b = (k_b/d_b)$. The value of the conceptual path length, ($\mathbf{d_b}$), is unknown, but it remains constant. When we also assume that the flow of heat remains essentially constant along each of the paths in **Fig. 15-4b**, we can write

$$(\text{Constant heat flow})(\text{constant } d_b) = k_b\,(T_c - T_{sk}) = k_b\,(dT) \qquad (15\text{-}1b)$$

for all values of ($\mathbf{T_{op}}$) and their associated values of ($\mathbf{T_{sk}}$). Now, when ($\mathbf{T_{op}}$) changes, and ($\mathbf{T_{sk}}$) changes in the same direction, while ($\mathbf{T_c}$) remains constant, then ($T_c - T_{sk}$) changes in the opposite direction. To maintain the constancy of flow, ($\mathbf{k_b}$) will have to change in the same direction as ($\mathbf{T_{op}}$) and ($\mathbf{T_{sk}}$). In other words, ($\mathbf{k_b}$) rises and falls with ($\mathbf{T_{op}}$), increasing in a warming environment and decreasing in a cooling environment. Furthermore, in a very general sense the relationship between ($\mathbf{k_b}$) and ($T_c - T_{sk}$) will be in the form of an hyperbola. As we will see in **Box 15-1**, this form of the relationship for human beings is borne out, approximately, by experimental evidence.

The manner of change in ($\mathbf{k_b}$) just described is the essence of the variable cardiovascular system. An increasing ($\mathbf{k_b}$) results primarily from *vasodilation* as the blood capillaries just beneath the skin *dilate* and increase in diameter. Similarly, a decreasing ($\mathbf{k_b}$) results primarily from *vasoconstriction*. Vasodilation is usually accompanied by an increase in the heart rate, which further increases the rate at which heat is carried from the core to the skin, from where it is deposited in the environment. Vasoconstriction is usually accompanied by a decrease in the heart rate, and body heat is thereby conserved.

Some changes in the thermal conductivity of an animal's hair or feather coat take place in a manner similar to the changes in ($\mathbf{k_b}$). These can occur rapidly and in response to an error signal as described earlier, such as when the hairs or the feathers become erect — stand away from the skin. Longer-term changes take place as the coat becomes seasonally thinner and thicker by the loss and re-growth of some of its elements.

The thermal resistance of a haircoat depends primarily on it's thickness. However, since both the density and shape of individual fibres in the coat and the speed of externally moving air[3] can change the coat's insulative characteristics, no simple relationship covering all situations will model the resistance with precision. All the same, for the purposes of modeling an animal's energy balance to an acceptable degree of accuracy, we have developed a numerical module for resistance based on the contents of a well-known graph[4]

depicting resistance measured in the laboratory as a function of coat thickness for a wide range of fur-bearing animals. A simplified version of this graph appears as **Fig. 15-5**. In the original presentation, several data points represent each of the index numbers found in **Fig. 15-5**, no doubt describing a variety of combinations of animal age, season, wind speed, and so on. In **Fig. 15-5** we have placed an index number near the center of the scatter of data points for each of the animal types in the original.

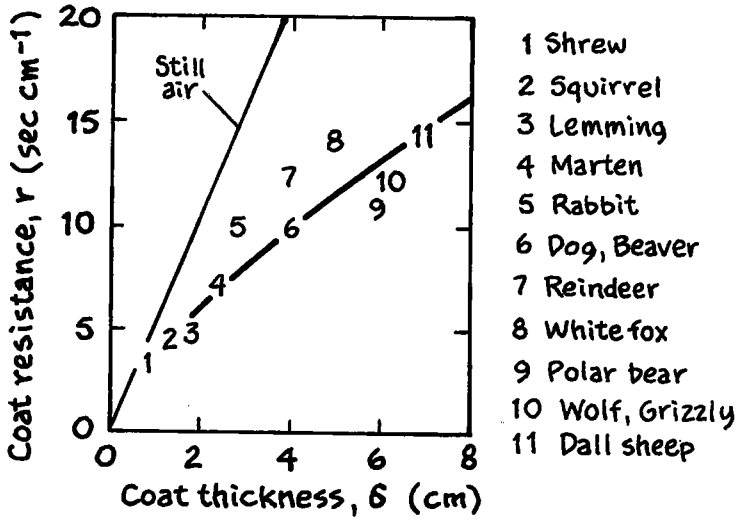

Fig. 15-5 The thermal resistance of a hair coat is systematically related to the thickness of the coat, as shown for a sample of fur-bearing animals[4]. Also see **Box 15-2**.

The module we have developed for thermal resistance consists of several regression models connecting the coat thickness, (**d**); the thermal resistance of the coat, (**r**); the animal's mass, (**W**); and the value of (**r**) expressed as a percent of the resistance for still air, (**p**). We have introduced the animal's mass by using the procedure of "sizing" described in **Footnote (O)** of **Chapter 13**. The first model — **Eq.(15-2a)** — is depicted by the heavy line in **Fig. 15-5**:

$$r = 3.7\ (d)^{0.72} \qquad (15\text{-}2a)$$

where $\{r\}$ = (sec cm^{-1}) and $\{d\}$ = (cm). From the same data set we obtain:

$$r = 6.8\ (W)^{0.17} \qquad (15\text{-}2b)$$

$$d = 2.6\ (W)^{0.24}, \text{ and} \qquad (15\text{-}2c)$$

$$p = 0.59\ (W)^{-0.052} \qquad (15\text{-}2d)$$

with the same units for (**r**) and (**d**), and $\{W\}$ = (kg)[4]. These three alternative regression models complete the module for characteristics of a large animal's coat.

Evaporative cooling in a large animal

Breathing carries both sensible and latent heat directly from the body core to the environment. A large animal at rest and under no hyperthermal stress will dissipate between 5 and 10 percent of its basal metabolic heat energy through the heat exchange of breathing and, in the case of a coatless animal, an additional small fraction will be lost through evaporation from the skin. Beyond these basal losses, many animals use panting and evaporative cooling through sweating as short-term emergency measures for thermoregulation. While sweating is very effective and efficient in the short run, there is an upper limit on the rate at which water can be delivered to the skin surface. Further, reliance on sweating is often limited by the availability of water for renewing the body's supply. The information we offer now is based mainly on observations of human beings, but the general principles apply to many large animals that use sweating for thermoregulation.

As we have noted, sweating is triggered by the sensing of a positive error signal, and the rate at which sweat is delivered to the skin surface is proportional to the size of the error signal[5]. In fact, for most large animals, including human beings, the maximum rate of water delivery is attained within less than 0.5 °C above the set point. The notion of a rapid rise in the sweat rate, (**SR**), when the body temperature exceeds a set point is exhibited in several forms in **Fig. 15-6**, which are based on the data[6] in **Table 15-2**.

All three panels of **Fig. 15-6** exhibit a dependence of (**SR**) in a human male on one of the body temperatures. By appropriate construction of the temperature scales we have made the slopes similar in all three panels; whereas, in reality they are not similar. When we

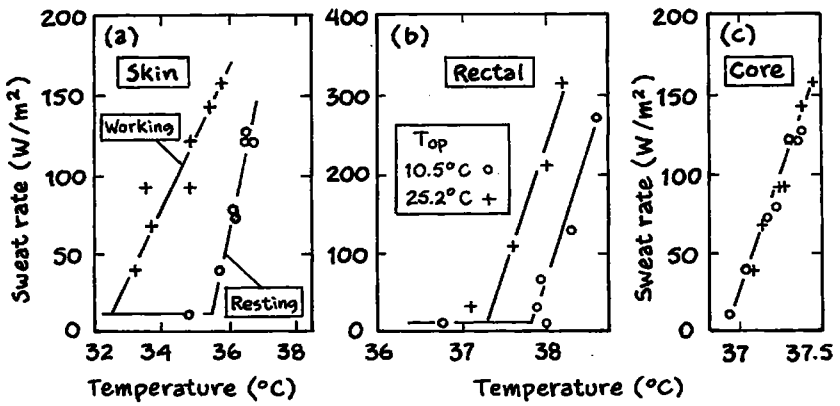

Fig. 15-6 The observed rate of sweating, (**SR**), for a human male is well correlated with the observed metabolic work rate, (**M**), and the several body temperatures considered in the previous sections. **(a)** It is related to the skin temperature, (T_{sk}), as modulated by (**M**). **(b)** It is related to the rectal temperature, (T_{re}), as modulated by the operative temperature, (T_{op}). **(c)** Sweating is triggered by an error signal in the core temperature, (T_c), which determines the rate, (**SR**).

assume the expression (SR) = (T_{20}) + B(T), where (T_{20}) is the set point temperature at which (**SR**) first rises above the basal rate of 20 (Wm^{-2}), then, with linear regression analyses, we obtain approximately these differences among the models in **Fig. 15-6**:

Primary predictor	Secondary predictor	(T_{20}) (deg C)	Slope (B) ($Wm^{-2}deg^{-1}$)	Data
Skin (T_{sk})	Working: M ≈ 5 Wm^{-2}	32.6	31.	Table 15-2, Set B, lines 18-24
	Resting: M ≈ 2 Wm^{-2}	35.6	102.	Table 15-2, Set B, lines 11-16
Rectal (T_{re})	T_{op} = 25.2 deg C	37.3	312.	Table 15-2, Set A, lines 1, 2, 4, 5, 8-10
	T_{op} = 10.5 deg C	37.9	312.	Table 15-2, Set A, lines 1, 2, 4, 5, 8-10
Core (T_c)	None needed	37.0	296.	Table 15-2, Set B, lines 11-24

In **Fig. 15-6a** it is clear that, for a given value of ($\mathbf{T_{sk}}$), the sweat rate is larger when the subject is working than when he is resting. A less obvious interpretation is that sweating is initiated at a lower value of ($\mathbf{T_{sk}}$) when the subject is working than when he is resting. The two lines in **Fig. 15-6a** converge near the sweat rate that equals the metabolic rate, as will be verified in the following section on mathematical modeling of the energy balance of a large animal. A similar analysis for **Fig. 15-6b** shows that, for a given value of ($\mathbf{T_{re}}$), the sweat rate is larger when the environment is warm than when it is cool; and that sweating is initiated at a lower value of ($\mathbf{T_{re}}$) when the environment is warm. An analysis for **Fig. 15-6c** shows that the relationship between ($\mathbf{T_c}$) and (**SR**) is not affected by either ($\mathbf{T_{op}}$) or (**M**).

A brief summary of this analysis of the sweat rate in Man is that an estimate of (**SR**) based primarily on the *external* variable determined mainly by the environment — ($\mathbf{T_{sk}}$) — must be modulated by an *internal* variable whose value is determined mainly by the activity level of the subject: (**M**). On the other hand, an estimate of (**SR**) based primarily on the *internal* variable determined mainly by the activity level — ($\mathbf{T_{re}}$) — must be modulated by an *external* variable whose value is determined mainly by the environment: ($\mathbf{T_{op}}$). In contrast, an estimate of (**SR**) based on ($\mathbf{T_c}$) is unmodulated by any other variable. A final generalization is that the sweat rate is as much as nine times as responsive to an internal temperature change — in ($\mathbf{T_c}$) or ($\mathbf{T_{re}}$) — as it is to an external temperature change — in ($\mathbf{T_{op}}$).

A useful way to consider the rate of sweating is as a multiple of some reference value, such as the basal or the working metabolic rate, so that (SR/M_b) or (LE/M) becomes the measure of the sweat rate. We commented earlier that there is a maximum rate at which the body can deliver sweat to the skin even when the supply of body water is plentiful. While investigating human responses to extreme conditions such as those found in military and industrial environments, Douglas Lee and his colleagues considered the rate of sweating as a multiple of the maximum rate of sweating possible under the ambient environmental conditions, ($\mathbf{SR_{max}}$).

Lee and his colleagues borrowed terminology from mechanical engineering when they referred to the conditions that force a response as

the *stress* and to the responses themselves as the *strain*. Further, they used the term *relative strain*, (**RS**), to refer to the sweat rate required for thermal equilibrium *relative* to the maximum rate possible under the ambient environmental conditions[7]. Thus, when the rate required, ($\mathbf{SR_{req}}$), exactly equals the largest rate possible, ($\mathbf{SR_{max}}$), then RS = $(SR_{req})/(SR_{max})$ = 1.

In **Fig. 15-7** we present a simplified version of Lee's calculated results[D] by placing lines of equal (**RS**) on the TRe diagram. **Fig. 15-7a** presents these lines for a breed of cow with limited physiological and anatomical ability to sweat — native to regions outside the tropics — and **Fig. 15-7b** presents the lines for a breed of cow with a greater ability — a "tropical" cow. For the former, the maximum rate of delivery that is physiologically and anatomically possible, ($\mathbf{SR_{max}}^*$), is 148 Wm^{-2}, while for the latter it is 295 Wm^{-2}. **Fig. 15-7c** presents the lines for a typical human male, with a maximum possible delivery rate of 379 Wm^{-2}. In the Figure, these three values of ($\mathbf{SR_{max}}^*$) are associated with the horizontal dashed lines marking the location of the kinks in lines of equal (**RS**). In all three panels, the dotted areas represent combinations of environmental heat and moisture that require evaporative cooling in excess of the maximum possible. In these areas, therefore, the hyperthermal stress cannot be tolerated for long periods.

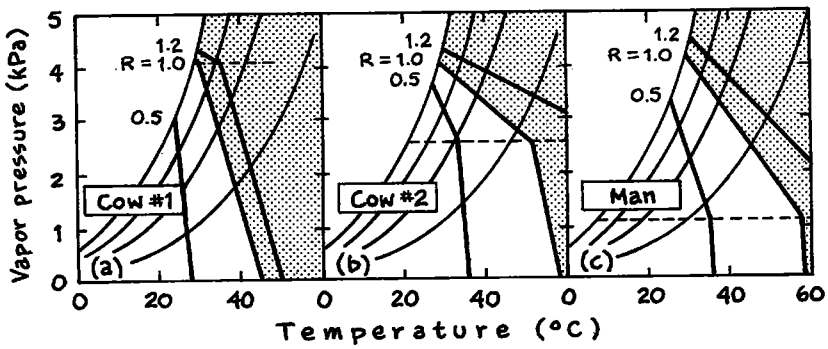

Fig. 15-7 The concept of relative strain is presented as lines of equal (**RS**) on the coordinates of the TRe diagram. Cow #1 **(a)** is an extratropical breed, while Cow #2 **(b)** is a tropical breed possessed of an enhanced ability to deliver sweat to the skin. **(c)** A typical human male has an even greater ability than Cow #2. In all three panels, the dotted areas represent combinations of environmental heat and moisture that require evaporative cooling in excess of the maximum possible.

It is important to note that the maximum rate of delivery that is physiologically possible, ($\mathbf{SR_{max}}^*$), is different from, but may be equal to, ($\mathbf{SR_{max}}$). That is, ($\mathbf{SR_{max}}^*$) is physiologically determined while ($\mathbf{SR_{max}}$) is environmentally determined as long as ($\mathbf{SR_{max}}$) $\leq$ ($\mathbf{SR_{max}}^*$).

(D) For comparison, refer to the sweat rates in **Fig. 15-6**.

Mathematically, (**RS**) = ($\mathbf{SR_{req}}$)/($\mathbf{SR_{max}}$). As we consider in **Box 15-1**, ($\mathbf{SR_{max}}$) may be represented by

$$SR_{max} = (H_w)[e_{s(sk)} - R\ e_{s(op)}] \qquad (15\text{-}3)$$

where ($\mathbf{H_w}$) is a suitable transfer coefficient; ($\mathbf{e_{s(sk)}}$) is the saturation vapor pressure at the temperature of the wet skin, ($\mathbf{T_{sk}}$); (**R**) is the ambient relative humidity; and ($\mathbf{e_{s(op)}}$) is the saturation vapor pressure at ($\mathbf{T_{op}}$).

With these definitions in mind, and to clarify further the relationships depicted in **Fig. 15-7**, we will explain the configuration of the lines of equal (**RS**): a decreasing (**R**) as ($\mathbf{T_{op}}$) increases, with a kink at a certain value of vapor pressure. Begin by tracing a line of equal (**RS**) from the point where it intersects the curve of saturation vapor pressure: R = 100%. The numerator and the denominator of (RS) = (SR_{req})/(SR_{max}) are both increasing by the same amount for each increase in ($\mathbf{T_{op}}$), because (**RS**) is constant on the line we are tracing. The numerator, ($\mathbf{SR_{req}}$), increases because the body is under greater thermal stress. The explanation for the increase in the denominator, ($\mathbf{SR_{max}}$), is less direct.

As shown in **Fig. 15-4**, ($\mathbf{T_{sk}}$) increases as ($\mathbf{T_{op}}$) increases. Thus, the vapor pressure of the skin, ($\mathbf{e_{s(sk)}}$), also increases as ($\mathbf{T_{op}}$) increases. Because the denominator — which is $(H_w)[e_{s(sk)}\text{-}Re_{s(op)}]$ according to **Eq.(15-3)** — must increase by the same amount as ($\mathbf{SR_{req}}$); and because ($\mathbf{e_{s(sk)}}$) increases with ($\mathbf{T_{op}}$) less rapidly than does ($\mathbf{e_{s(op)}}$), keeping the ratio constant requires a decrease in (**R**). Thus, an increase in ($\mathbf{T_{op}}$) requires a decrease in (**R**) for maintenance of a constant (**RS**). Eventually, the denominator is equal to the value of the physiological limit, ($\mathbf{SR_{max}}^*$). It cannot increase more. Any increase in ($\mathbf{T_{op}}$) results in an increase in the numerator but none in the denominator: an increase in (**RS**). When the denominator increases to the value of ($\mathbf{SR_{max}}^*$), we have reached the largest temperature for which (**RS**) has the value we have been following, and the value of that temperature is essentially the same for all smaller values of (**R**). This condition is shown in **Fig. 15-7** below the kink in the line of constant (**RS**).

Among different animals, the maximum tolerable temperature — where the kink occurs — increases as ($\mathbf{SR_{max}}^*$) increases. Taking values from Lee's diagram in **Fig. 15-7** we see, for example when SR = 1, that

for cow #1 with (SR_{max}^*) = 148 Wm^{-2} the largest (T_{op}) $\approx$ 32 °C;

for cow #2 with (SR_{max}^*) = 295 Wm^{-2} the largest (T_{op}) $\approx$ 53 °C; and

for the Man with (SR_{max}^*) = 379 Wm^{-2} the largest (T_{op}) $\approx$ 58 °C.

Note that, in the three panels, below the kinks, the line for a given value of (**RS**) is not quite vertical. This is because the denominator can increase slightly more at higher temperatures, not by sweating but by an increase in the depth and rate of breathing, or panting. If pant-

ing behavior is precluded, a line of constant (**RS**) would be vertical below the kink. Cow #1 shows a greater ability to lose heat through panting than does Cow #2, and both show a greater ability than does the Man.

We offer further analysis of the concept of Relative Strain in **Box 15-1**, where we adopt a form of presentation slightly different from the one used by Lee. This alternative is illustrated in **Fig. 15-8** where the ordinate is relative humidity, (**R**), rather vapor pressure, (**e**), as in the TRe diagram. We have adopted this alternative because it gives the same perspective for both very moist and very dry environments, even though this form sacrifices the convenience of straight lines for values of (**RS**).

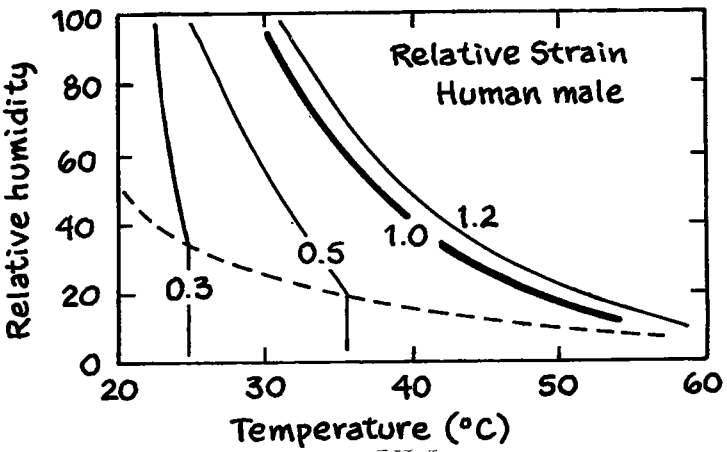

Fig. 15-8 The information presented for a human male in **Fig. 15-7c**, on the rate of sweating, (**SR**), expressed as a value of relative strain, (**RS**), is presented here on coordinates of temperature and relative humidity. Both the lines of equal (**RS**) and the dashed line associated with the kinks in those lines have different orientations after the change of coordinates from those in **Fig. 15-7**. See also the analyses of **Box 15-1**.

We close this section by noting that observations in a controlled experimental environment have shown that both (**SR**) and ($\mathbf{SR}_{max}$*) usually change with time during prolonged, concerted exercise, and that the value of (**SR**) depends on whether the subject is permitted free access to drinking water. In one set of experiments, with subjects who worked hard for five hours in a very hot environment, Wyndham *et al.* observed that the physiological limit, ($\mathbf{SR}_{max}$*), declined from about 765 to 330W from the first to the fifth hour. In another set of experiments, with subjects walking continually on a treadmill for six hours at a speed of 5.6 km hr^{-1} in an environment with T_{op} = 31°C, Sargent *et al.* observed that, (i) for those with free access to drinking water, (**SR**) rose from 285W at the end of the first hour to 460W at the end of the second hour, declining to 415W from the second to the fifth hour; but that, (ii) for subjects without free access to drinking water, (**SR**) rose from 245W at the end of the first hour to only about 375W, a rate that remained essentially constant from the second through the fifth hour[8].

The structure and use of a model for the energy balance of a large animal

The modeling of biometeorological energy balances, in conjunction with experimental observations made in controlled environment laboratories, began in the United States in the 1950s with the work of scientists at the Pierce Laboratory of Yale University. The attention of Gagge and Stevens working at Pierce was focused on the basic physiology of thermoregulation in Man. Their work was extended in the following decade by scientists employed by the Quartermaster Corps of the United States Army, who were primarily interested in the military implications of the basic physiology of thermoregulation in Man for equipment and clothing design, especially under conditions of extreme temperature[9].

Following shortly after the efforts to model the energy balance of Man came those of Gates and his students, in the 1960s, to model small animals and birds. In their pioneering and classic study in modeling the behavioral thermoregulation of a small lizard, Bartlett and Gates (1967) shifted from their practice in modeling leaves by treating the surface areas of energy exchange expliciltly. In later efforts, however, Gates's group reverted to treating the surface areas implicitly in an animal model applied to the concept of Climate Space (Porter and Gates, 1969). We are unaware of coordinated and systematic efforts to model the energy balance of large animals other than that of Curtis (1981), whose major concern was with management of the thermal environments of swine to optimize success in reproduction and meat production[10].

In simplest terms, the questions asked of a model of the energy balance of a small animal generally flow from the knowledge that the animal employs a system of thermoregulation in which fine tuning is achieved by means of a variable metabolic rate operating in the presence of an essentially constant thermal resistance to the transfer of heat into and out from the body core. The questions asked of a model for large animals, on the other hand, are usually based on a system in which thermoregulation is achieved by means of a variable thermal resistance to the transfer of body heat in the presence of an essentially constant metabolic rate.

Models of the energy balance of a small animal and of a large animal differ mainly in the operation of certain terms, rather than because of differences in the structure of the model. The models do differ somewhat in structure, however, as well as having similarities, as indicated by **Tables 14-1** and **15-4**. We have just mentioned the principal differences in operation: variability of the thermal resistance to the flow of body heat is important in models of a large animal but not in models of a small animal; whereas, variability of the metabolic rate is important for a small animal but not for a large animal.

There are two principal differences in structure. The first pertains to the surface areas through which energy is exchanged with the animal's environment. Models for a small animal usually accept information about energy flux density in units of {energy/area}, with the area — taken to be a "typical unit of area" — being implicit rather than explicit. In models for a large animal, on the other hand, information about energy flux density is in units of {energy} multiplied by {area}, the areas being calculated explicitly(E). The second difference in structure is that the modeling of evaporative cooling by a large animal is usually distinctly more explicit and detailed than for a small animal. In particular, the structure of the model for a large animal separates evaporative cooling related to breathing from that related to sweating.

The areas involved in a model of the energy balance

In models for the energy balance of larger animals, account is usually taken of the fact that the various parts of the surface area are involved in the different radiant, convective, and conductive exchanges of energy between the animal and its environment. An obvious example, discussed next, is the difference in areas involved in the absorption of direct and of indirect, or diffuse, shortwave radiation in the out-of-doors. A second example is its area of direct, solid contact with the ground.

In what follows we refer to the entire surface area as the *Total Area*, (**A**), and to the area in contact with the substrate as the *Contact Area*, ($\mathbf{A_c}$). The area through which the exchange of direct shortwave radiation takes place is equal to the area of the shadow cast by the animal. Accordingly, it is called the *Shadow Area*, ($\mathbf{A_d}$). The convective exchanges and the exchanges of longwave and diffuse shortwave radiation take place through the *Extended Area*, ($\mathbf{A_e}$). Approximately, $A_e = (A - A_c)$. The principal advantages for using these differentiated areas lie in the possibilities to model (i) postural effects with respect to sun and wind, (ii) effects of various degrees of contact with the substrate, (iii) differences between quadrupeds and bipeds in the same environment, and (iv) effects of changes in orientation to sun and wind by a quadruped. We will illustrate several of these kinds of effect presently.

We begin our presentation of modeling the energy balance of a large animal with **Fig. 15-9**, which displays the essential details for estimating the area that intercepts direct solar radiation: the "shadow

(E) In this Volume we follow the general rule of implicit areas for small animals and explcit areas for large animals, including Man. There are, however, a few notable exceptions to this rule in the biometeorological literature. Gates, early in his marvellously successful program to model plants and animals, went to great pains to deal explicitly with areas of coniferous tree branchlets (for example, see Tibbals *et al.*, 1964) and of a small lizard (Bartlett and Gates, 1967). As we have noted, however, he dealt implicitly with areas in most of the work associated with development of the concept of Climate Space.

area, (A_d)." Following the Figure we include **Table 15-3** in place of a formal derivation of each of the eight areas used in the model we will present. In addition to the eight submodels given in the Table, we include there heuristic validations of them with values of 0° and 90° for each of the angles involved. We have followed a practice familiar to biometeorologists whereby animals are modeled as right cylinders, with vertical axes for bipeds and horizontal axes for quadrupeds. For reasons that are more than simply whimsical, we refer to these cylindrical models as "beer can models", as clarified in **Box 15-1**.

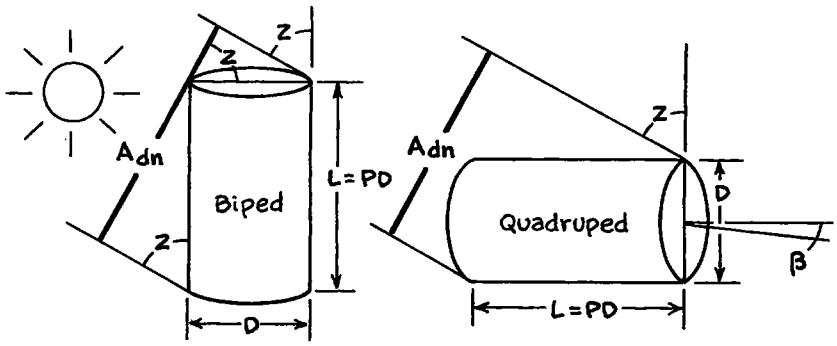

Fig. 15-9 The basic representation of the terms involved in estimating the shadow area, (A_{dn}), cast by a large animal on the plane normal to the solar beam. The estimation involves the solar zenith angle, (**Z**), for both models. For a bipedal animal, the direction that the model faces does not matter. For a quadrupedal animal, however, the estimation involves the angle, (β), between the axis of the cylinder and the horizontal projection of the solar beam.

Fig. 15-10 exhibits the results of calculations of the shadow area cast on a surface normal to the solar beam, (A_{dn}), for cylindrical models of a biped and a quadruped with dimensions Length = 3x Diameter. The shadow areas, calculated for 40°N latitude, are all expressed as a percent of the total surface area of the beer can: 100 (A_{dn}/A). In both panels of **Fig. 15-10** we see that the fractional area, for a quadruped whose axis is aligned perpendicular to the solar beam (β = 90°), is 27% regardless of the hour or the season. What is more, again in both panels of **Fig. 15-10**, we see that the fractional area for an animal "curled into a ball" — represented by a sphere with the same weight — is 20.5% regardless of the hour or the season.

In **Fig. 15-10a** we note that in winter a biped, with a vertical axis, intercepts a larger amount of direct shortwave radiation than does a quadruped, with a horizontal axis, or a sphere, regardless of hour. That is primarily because the rays of the low winter sun are, at all hours, more nearly perpendicular to the body of a biped than to the body of a quadruped. In **Fig. 15-10b** we note that between 10h and 14h in summer, however, a biped intercepts a smaller amount of direct shortwave radiation than does a sphere or a quadruped, regardless of its orientation to the sun. Except for these hours in summer,

TABLE 15-3 SUBMODELS FOR AREAS INVOLVED IN A BEER CAN MODEL OF THE ENERGY BALANCE OF A LARGE ANIMAL

SUBMODELS

Animal	Cylinder sides	End	Submodel[a] Area
Biped			
Total, A	$2\pi L(D/2)$	$2\pi(D/2)^2$	$(P + ½)(\pi D^2)$
Contact, A_c	-	$\pi(D/2)^2$	$(¼)(\pi D^2)$
Extended, A_e	$2\pi L(D/2)$	$\pi(D/2)^2$	$(P + ¼)(\pi D^2) = (A - A_c)$
Shadow, A_{dn}	L sinZ	$\pi(D/2)^2 \cos Z$	$[P \sin Z + (\pi/4) \cos Z](D^2)$
Quadruped			
Total, A	$2\pi L(D/2)$	$2\pi(D/2)^2$	$(P + ½)(\pi D^2)$
Contact, A_c	-	-	Fraction of A
Extended, A_e	-	-	$A - A_c$
Shadow, A_{dn}	$L(1 - \sin^2 Z \cos^2\beta)^{½}$	$\pi(D/2)^2 \sin Z \cos\beta$	$\{[(\pi/4)\sin Z \cos\beta] + [P(1-\sin^2 Z \cos^2\beta)]\}D^2$

HEURISTIC VALIDATION OF SHADOW AREAS

Animal	Z	b	Validation
Biped, A_{dn}	0°	-	$[P(0) + (\pi/4)(1)](D^2) = (\pi/4)(D^2)$
	90°	-	$[P(1) + (\pi/4)(0)](D^2) = LD = PD^2$
Quadruped, A_{dn}	0°	0°	$\{[(\pi/4)(0)(1)] + [P(1 - (0)(1))]\}D^2 = LD = PD^2$
	0°	90°	$\{[(\pi/4)(0)(0)] + [P(1 - (0)(0))]\}D^2 = LD = PD^2$
	90°	0°	$\{[(\pi/4)(1)(1)] + [P(1 - (1)(1))]\}D^2 = (\pi/4)(D^2)$
	90°	90°	$\{[(\pi/4)(1)(0)] + [P(1 - (1)(0))]\}D^2 = LD = PD^2$

NOTES:
(a) In the text the diameter of the model cylinder is D while the height or length of the model is L = PD.
(b) The derivation of the term $L(1 - \sin^2 Z \cos^2 b)^{½}$ is in **Appendix E**.

the sphere presents the smallest area for interception of direct sunlight. The actual radiant heat load, of course, requires multiplication of the shadow area by the direct shortwave flux density, ($\mathbf{S_d}$).

As shown in **Fig. 15-11**, the shadow cast on a horizontal surface — for example, a pavement — is $A_{dh} = A_{dn}/\cos Z$, and the direct solar radiant heat load is $(A_{dn}/\cos Z)x(S_h) = (A_{dn})x(S_n)$, since $S_h = S_n \cos Z$. If the surface on which the shadow is falling is vertical — for example, a wall — the area is $A_{dv} = A_{dn}/\sin Z$, where (**Z**) is the solar zenith angle. On that vertical surface, the direct solar radiant heat load is $(A_{dn}/\sin Z)x(S_v) = (A_{dn})x(S_n)$, since ($\mathbf{S_v}$), the flux density of direct solar radiation on the vertical surface, is $S_v = S_n \sin Z$. Finally, if the surface on which the shadow is falling is normal to the solar beam, the area of the shadow is (A_{dn}), and the radiant heat load from direct solar radiation is $(A_{dn})x(S_n)$, where ($\mathbf{S_n}$) is the flux density of direct solar radiation on the same surface. Thus, the direct solar radiant heat load is the same regardless of the orientation of the surface.

Mathematical modeling of the energy balance of a large animal

As in **Chapter 14**, before developing a model for the energy balance of a large animal we present a table setting out its charac-

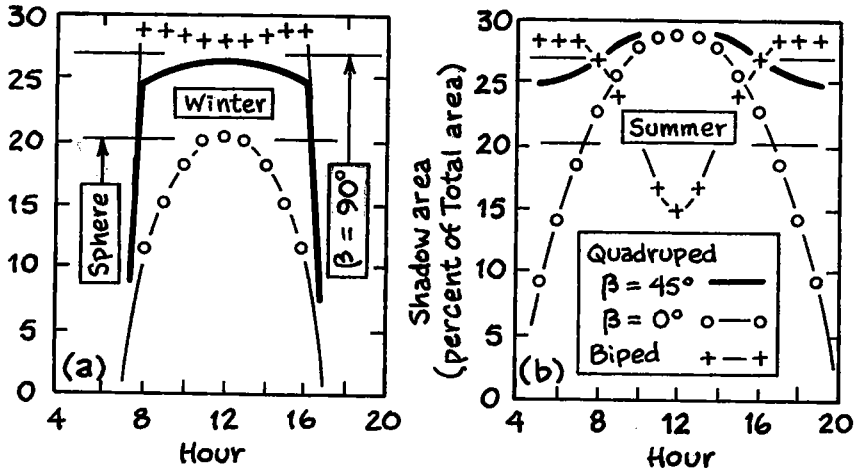

Fig. 15-10 Calculations of the shadow area for a "beer can" model of a large animal exhibit clearly the importance of posture and orientation in determining the animal's shortwave radiant heat load. The model's proportions are Length = 3xDiameter, and the areas are expressed as a percent of the total surface area of the can. The solar geometry is for **(a)** 15 January and **(b)** 30 June at 40°N latitude. When the quadruped's axis is perpendicular to the solar beam — the horizontal line marked (b = 90°) — the shadow area is the same (27%) regardless of the hour or the season, as is the case (20.5%) when the animal curls into a ball — a sphere of the same weight, as shown by the horizontal line marked (sphere).

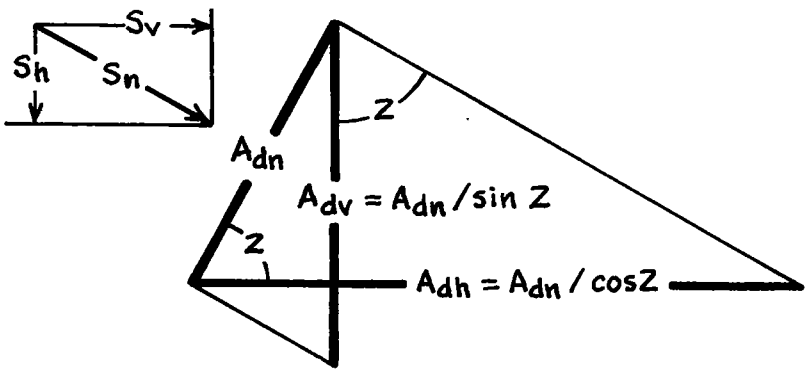

Fig. 15-11 Geometric relationships, for a surface on which a shadow is cast by a cylindrical model, demonstrate that the direct solar radiant heat load on the model casting the shadow is the same regardless of the orientation of the surface.

teristics. The model for large animals has three principal differences from that for small animals used in **Chapter 14**. The first, as we have already noted, is the treatment of energy fluxes according to the areas through which the fluxes take place. The second is the separation of the coat from the body, with the thermal resistances of the two being specified separately. The third principal difference is the use of the term (Δ), which we initially consider simply as the rate of withdrawal of heat from the body core or from the body mass

required to make the model balance. Thus, the body is in thermal equilibrium when $\Delta = 0$. The term (Δ) will be described in greater detail below, as part of several applications of the model.

The derivation and use of our model for large animals, and especially Man, follows closely the sequence for small animals presented in **Chapter 14**, including the use of the synthetic temperature we refer to as the *operative temperature*, $(\mathbf{T_{OP}})^{(F)}$. As noted in the preceding section, we make use of a cylindrical shape for large animals: a vertical cylinder to represent bipedal animals, including Man, and a horizontal one for quadrupedal animals. The counterpart of **Table 14-1** in this chapter is **Table 15-4**, in which the reader may keep track of the formulation of the basic model for the energy balance of large animals.

TABLE 15-4 CHARACTERISTICS OF THE MODEL FOR THE ENERGY BALANCE OF A LARGE ANIMAL

Energy stream	Modeled characteristics	Comment
Shortwave Flux, direct	Flux per unit area (see text)	Appears as ($\mathbf{S_d}$)
Shortwave Flux, diffuse	Flux per unit area (see text)	Appears as ($\mathbf{S_e}$)
Shortwave absorptivity	Appears as ($\mathbf{a_s}$)	Same for direct and diffuse
Metabolic heat	Total flux or flux per unit area (see text)	Appears in (M - LE)
Evaporation from core	Decrement from the metabolic flux	Appears in (M - LE)
Conduction through body	Flux per unit area per degree	Transfer coefficient ($\mathbf{h_b}$)
Thickness of body	Fraction of dimension, (**D**)	-
Conduction through coat	Flux per unit area per degree	Transfer coefficient ($\mathbf{h_f}$)
Thickness of coat	Fraction of dimension, (**D**)	-
Net longwave, surface	Flux per unit area per degree	Transfer coefficient, ($\mathbf{h_r}$)
Net sensible, surface	Flux per unit area per degree	Transfer coefficient, ($\mathbf{h_c}$)
Net latent, surface	Decrement from the metabolic flux	Appears in (M - LE)
Conduction to substrate	Flux per unit area per degree	Transfer coefficient, ($\mathbf{h_g}$)
Area, total for the body	See text for formulation	Appears as (**A**)
Area, shortwave direct	See text for formulation	Appears as ($\mathbf{A_d}$)
Area, shortwave diffuse	Total minus contact area	Appears as ($\mathbf{A_e}$)
Area, longwave exchange	Total minus contact area	Appears as ($\mathbf{A_e}$)
Area, net sensible	Total minus contact area	Appears as ($\mathbf{A_e}$)
Area, net latent	Not modeled separately	Appears in (M - LE)
Area, contacting substrate	Fraction of total area	Appears as ($\mathbf{A_c}$)

Fig. 15-12, similar in several respects to **Fig. 14-31**, depicts the essential relationships to be considered in modeling the energy balance of a large animal exposed to the air and in contact with a substrate. As in **Chapter 14**, the cooling involved in breathing — both sensible and latent — is included as a simple decrement to the metabolic heat rate, so that the *net metabolic rate* is (M-LE). Again as in **Chapter 14**, we begin our analysis with a partitioning of the streams of the energy balances for (i) the inner surface C between the core and the body, (ii) the surface S between the body and the insul-

(F) We use the symbol ($\mathbf{T_{op}}$) for the operative temperature of a small animal's environment and ($\mathbf{T_{OP}}$) for that of a large animal's environment. The latter includes area-weighted temperatures while the former does not.

ating coat, and (iii) the outer surface X between the coat and the ground-air environment. The formulations make use of transfer coefficients, (**h**), as discussed in **Box 9-3** of **Volume 1** and in connection with **Fig. 14-31**.

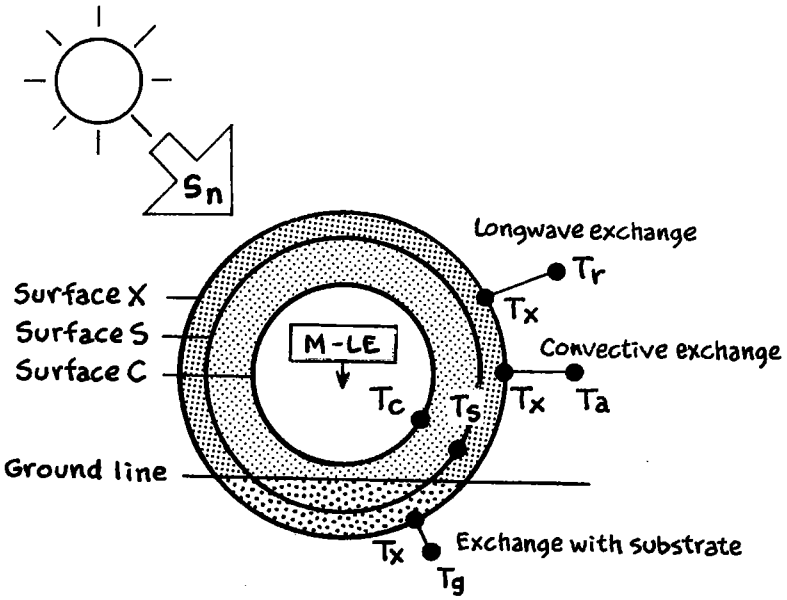

Fig. 15-12 The basic representation of the terms involved in the energy balance of a large animal consists of three concentric cylinders: the inner core, the body, and the coat. The three interfacing surfaces have temperatures of (T_c), (T_s), and (T_x), while external heat exchanges are with the sky, at temperature (T_r), with the air, at temperature (T_a), and with the substrate, at temperature (T_g). The net metabolic heat source, (M-LE), is in the core.

Surface and component	Inflow	Outflow
Inner core: surface C		
Net metabolic heat	$M + \Delta\text{-}LE$	-
Core-to-body surface conduction	-	$Ah_b(T_c - T_s)$
Body surface: surface S		
Core-to-body surface conduction	$Ah_b(T_c - T_s)$	-
Body-to-coat surface conduction	-	$Ah_f(T_s - T_x)$
Outer surface X		
Net direct shortwave radiant heat load	$a_s A_d S_d$	-
Net diffuse shortwave radiant heat load	$a_s A_e S_e$	-
Body-to-coat surface conduction	$Ah_f(T_s - T_x) = M + \Delta\text{-}LE$	-
Net longwave flux	-	$A_e h_r(T_x - T_r)$
Sensible convective flux to air	-	$A_e h_c(T_x - T_a)$
Sensible conductive flux to substrate	-	$A_c h_g(T_x - T_g)$

After we partition the streams, we adopt for simplicity the following terminology in combining the transfer coefficients with their respective areas:

$H_b = A\,(h_b)$; $H_f = A\,(h_f)$; $H_r = A_e\,(h_r)$; $H_c = A_e\,(h_c)$; and $H_g = A_c\,(h_g)$.

For reasons that will become apparent, we also include with the net metabolic rate the term (Δ), mentioned above, to represent a withdrawal of heat energy from storage in the animal's body. Finally, again for simplicity, we adopt the following for the shortwave budget:

$$a_s\,A'\,S' = a_s\,A_d\,S_d + a_s\,A_e\,S_e$$

From the balances for Surfaces C and S and solving for T_x, we obtain, as the analog for **Eq.(14-2a)**:

$$T_x = T_c - (1/H_b + 1/H_f)\,(M + \Delta - LE) \qquad (15\text{-}4a)$$

From the balances for Surfaces S and X, we obtain, as the analog for **Eq.(14-2b)**:

$$T_x = [a_s\,A'\,S' + (M + \Delta\text{-}LE)]/\Sigma H_e + [H_r T_r + H_c T_a + H_g T_g]/\Sigma H_e \qquad (15\text{-}4b)$$

where $\Sigma H_e = (H_r + H_c + H_g)$. Equating the two expressions for ($\mathbf{T_x}$) and rearranging yields the analog for **Eq.(14-3a)**:

$$T_c - T_{OP} = (a_s\,A'\,S'/\Sigma H_e) + (1/\Sigma H_e + 1/H_b + 1/H_f)\,(M + \Delta\text{-}LE) \qquad (15\text{-}5a)$$

where the operative temperature, $T_{OP} = (H_r T_r + H_c T_a + H_g T_g)/\Sigma H_e$, is a weighted mean of the radiant, air, and substrate temperatures. Defining the conductance parameter for a large animal, ($\mathbf{K_L}^*$), by $[1/\Sigma H_e + 1/H_b + 1/H_f] = (1/KL^*)$, rearrangement yields our basic calculating model for large animals, which plays the same role as **Eqs.(14-3b)** and **(14-3c)**:

$$\Delta = K_L^*[T_c - T_{OP} - (a_s\,A'\,S'/\Sigma H_e)] - (M - LE) \qquad (15\text{-}5b)$$

and for which $\Delta = 0$ is the condition of thermal equilibrium[11].

We continue this section with several illustrations of typical results obtained when using this model, supplemented by more extensive examples in **Box 15-1**. In **Fig. 15-4a** we explored, using experimental observations from a controlled laboratory environment, the systematic relationship between the skin temperature of a man, ($\mathbf{T_{sk}}$), and the operative temperature of the environment, ($\mathbf{T_{OP}}$), as modified by the metabolic work rate, (**M**). **Fig. 15-13** presents the results of calculations, made with the energy balance model just developed for a biped, of the same relationship. In particular, these results suggest that the effects of changes in several other variables can be quantified by means of the linear relationship

$$(T_{sk} - T_{OP}) = a + b\,(T_{OP})$$

where (a) and (b) are regression coefficients. These other variables whose effects we can quantify are the core temperature, ($\mathbf{T_c}$), and the flux density of direct shortwave radiation, ($\mathbf{S_d}$). The results from the model are set against the observational results, in the form of the error bars, from **Fig. 15-4a**. As intuition would suggest, (a) is directly proportional to ($\mathbf{T_c}$) and to ($\mathbf{S_d}$), and it is more sensitive to ($\mathbf{T_c}$) than

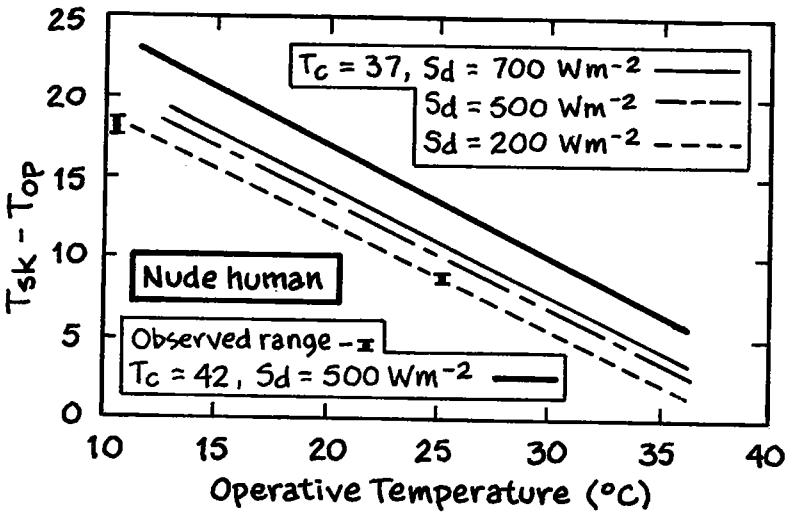

Fig. 15-13 Presented in the same form as in **Fig. 15-4a**, estimations of the skin temperature, (T_{sk}), of a large homeothermic biped, in thermal equilibrium with a prescribed environment, conform with observations, as evidenced by the error bars, from **Fig. 15-4a**.

The Animal		**The environment**	
Size (m): Diameter / Length	0.5 / 2.0	Direct shortwave flux, S_d (kW/m^2)	0.2, 0.5, 0.7
Core temperature, T_c (°C)	37, 42	Diffuse shortwave flux, S_n (kW/m^2)	0.1(S_d)
Metabolic rate: multiples of M_b (W)	1 See Note(a)	Air temperature, T_a (°C)	Various
Body conductivity, k_b (Wm^{-1}deg^{-1})	3	Sky temperature, T_r (°C)	T_a-15
Core-surface path, d_b (m)	0.3(D)	Ground temperature, T_g (°C)	Not used
Coat conductivity, k_f (Wm^{-1}deg^{-1})	100	Wind speed, U (m/sec) See Note(b)	1
Coat thickness, d_f (m)	0.001(D)	Solar zenith angle, Z	30
Coat shortwave absorptivity, a	0.7		
Latent heat loss rate, LE (Wm^{-2})	0.1(M)		

Notes:
(a) $M_b = 504.4\ (PD^3)^{0.75}$ (Watts) Use **Eq.(B13-4a)** with a sphere of density 10^3kg m^{-3}
(b) $h_c = 3.5(U/D)^{0.5}$ (Wm^{-2}deg^{-1}) See Constant C_6, **Table C-1.**

to ($\mathbf{S_d}$). Less obvious is the fact that (b) is essentially independent of both ($\mathbf{T_c}$) and ($\mathbf{S_d}$). In the calculations resulting in **Fig. 15-13**, we used **Eq.(15-5b)**, with the values of all system and environmental variables specified, varying only the thermal conductance of the body, ($\mathbf{h_b}$), until $\Delta = 0$. This equilibration simulated the vasomotor fine tuning accomplished by an animal's body in reaching thermal equilibrium. When the equilibration was accomplished, the model specified (T_{OP}) and ($T_{sk} - T_{OP}$) as outcomes. Without knowing the experimental circumstances in which the observations in **Fig. 15-4a** were obtained, our results in **Fig. 15-13** allow us to make the entirely reasonable inference that the illumination in the controlled laboratory was equivalent to about 200 Wm^{-2}.

In **Fig. 15-14** we examine the ranges over which a quadruped can possibly change its energy balance by altering its orientation to the

sun and the wind. On a typical winter morning in midlatitudes — **Fig. 15-14a** — the animal will experience the largest drain on its stored energy if it orients its axis parallel to the solar beam and perpendicular to the wind. In this position, according to the model, the animal will experience a withdrawal of stored energy at a rate 2.17 times its basal metabolic rate: $(\Delta/M_b) = +2.17$ (in the upper left

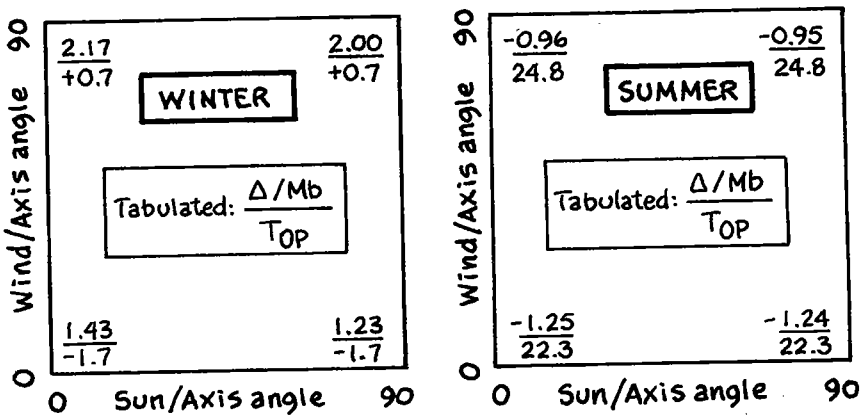

Fig. 15-14 While the ability of a quadruped to orient its body to the sun and the wind offers some opportunity to control its energy balance with the low sun and low temperature of a winter midday, there is much less opportunity with the high sun and high temperature of a summer midday. The relative thermal imbalance, (Δ/M_b) varys over the range of 2.17-1.23 — about 55% — in winter but only 1.24-0.95 — about 26% — in summer. See the text for further discussion.

The Animal		**The environment**	
Size (m): Diameter / Length	0.5 / 2.0	Direct shortwave flux, S_d (kW/m^2)	W=0.4;S=0.8
Core temperature, T_c (°C)	37	Diffuse shortwave flux, S_n (kW/m^2)	$0.1(S_d)$
Metabolic rate: multiples of M_b (W)	1 See Note(a)	Air temperature, T_a (°C)	W=5;S=30
Body conductivity, k_b (Wm^{-1}deg^{-1})	3	Sky temperature, T_r (°C)	T_a-15
Core-surface path, d_b (m)	0.3(D)	Ground temperature, T_g (°C)	Not used
Coat conductance, h_f (Wm^{-2}deg^{-1})	$10(h_b)$	Wind speed, U (m/sec) See Note(b)	5
Coat shortwave absorptivity, a	0.7	Solar zenith angle, Z	W=60;S=20
Latent heat loss rate, LE (Wm^{-2})	0.1(M)		

Notes:
(a) $M_b = 504.4\ (PD^3)^{0.75}$ (Watts) Use **Eq.(B13-4a)** with a sphere of density 10^3kg m^{-3}
(b) $h_c = 3.5(U/D)^{0.5}$ (Wm^{-2}deg^{-1}) See Constant C_6, **Table C-1.** D is wind travel distance across the body.

corner of the winter panel). The animal will experience the least drain on its stored energy if it orients its axis perpendicular to the solar beam and parallel to the wind, resulting in a withdrawal of stored energy at a rate only 1.23 times its basal metabolic rate (in the lower right corner of the winter panel). The maximum potential range of control by changing body orientation is about 55 percent[G]; but no orientation can, by itself, achieve thermal equilibrium at $\Delta = 0$ on a winter morning. Interestingly, the lowest operative tem-

(G) The figure of 55 percent is (2.17-1.23)/[(2.17+1.23)/2].

perature of T_{OP} = -1.7 °C is associated with the least drain on stored heat when Δ/M_b = 1.23. This is so because, when the body's microscale boundary layer is thickest, its energy balance is less closely coupled to the air temperature than to the sky temperature, which is 15 °C colder than the air temperature. That condition occurs whenever the axis of the cylindrical body is parallel to the wind direction and the length of wind travel past the body is greatest.

On a typical summer morning — **Fig. 15-14b** — the animal will experience the largest rate of increase in its stored energy if it orients its axis parallel to the wind. Note that its orientation to the high sun has almost no influence on the result. If the animal's body is oriented parallel to the wind, the animal will experience, according to the model, a rate of increase in body heat 1.25 times its basal metabolic rate: Δ/M_b = -1.25 (in the lower left corner of the summer panel). The animal will experience the lowest rate of increase if it orients its axis perpendicular to the wind, its orientation to the sun again being almost immaterial. In this position the animal will experience a rate of increase only 0.95 times its basal metabolic rate (in the upper right corner of the summer panel). The maximum potential range of control by changing orientation is only about 26 percent, and again no orientation can, by itself, achieve thermal equilibrium at Δ = 0.

Although we include in the model the capability for exchanging heat between the animal's body and the ground, we have not considered any such exchange in results presented up to this point. **Fig. 15-15** includes estimated effects for a quadruped lying down and having 15 percent of its total surface area in contact with the ground. In the calculations resulting in **Fig. 15-15**, we obtained a series of estimates of (Δ/M), which we call the *relative thermal imbalance*, for each of a range of environmental conditions with the animal standing. The range of environments contained differences in air temperature, in sky temperature, and in shortwave heat load. Then we made a second set of calculations for the same series of environments, each one resulting in a new value of (Δ/M), with the exception that the animal exchanges heat with the ground, at a soil temperature of 20 °C, through 15 percent of its total body surface area. Finally, we made a third set of calculations for the same series of environments, again with the animal exchanging heat with the ground, at a soil temperature now of 30 °C, again through 15 percent of its total body surface area.

If there were no effects due to heat exchange with the ground, all of the data points would lie on the line marked (1:1) in **Fig. 15-15**. Effects can be evaluated, therefore, as departures from that line. In hot environments, with large negative values of (Δ/M), the soil at (20 °C) has a cooling effect, according to the model calculations; but the effect is one of warming when its temperature is (30 °C). In cold environments, with relatively large positive values of (Δ/M), the soil has a warming effect at (20 °C), and a greater one at (30 °C).

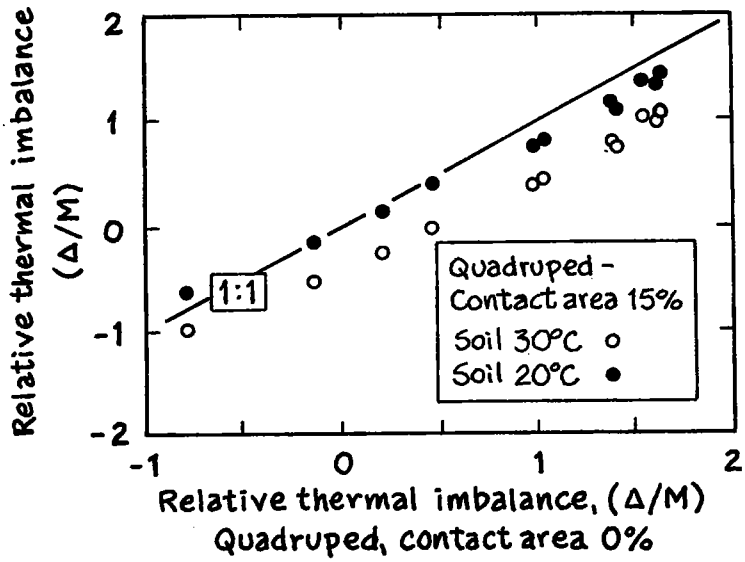

Fig. 15-15 The effect of heat exchange with the ground can be assessed by comparing the difference in the relative thermal imbalance, (Δ/M), between exposures in which exchange is taking place and exposures when no exchange is taking place. If exchange with the ground had no effect, all data points, obtained here by means of the model for energy balance, would fall along the line marked (1:1). In hotter environments with the most negative values of (Δ/M), the effect on (Δ/M) of the heat exchange may be cooling, turning to warming with warmer soil. In cold environments with large positive values of (Δ/M), however, the effect of the ground will be warming under a variety of circumstances.

The Animal		**The environment**	
Size (m): Diameter / Length	0.5 / 2.0	Direct shortwave flux, S_d (kW/m^2)	Various
Core temperature, T_c (°C)	37	Diffuse shortwave flux, S_n (kW/m^2)	0.1(S_d)
Metabolic rate: multiples of M_b (W)	1 See Note(a)	Air temperature, T_a (°C)	Various
Body conductivity, k_b (Wm^{-1}deg^{-1})	3	Sky temperature, T_r (°C)	T_a-15
Core-surface path, d_b (m)	0.3(D)	Ground temperature, T_g (°C)	20, 30
Coat conductance, h_f (Wm^{-2}deg^{-1})	1000(h_b)	Wind speed, U (m/sec) See Note(b)	1
Coat shortwave absorptivity, a	0.7		
Latent heat loss rate, LE (Wm^{-2})	0.1(M)		

Notes:
(a) $M_b = 504.4\ (PD^3)^{0.75}$ (Watts) Use **Eq.(B13-4a)** with a sphere of density 10^3kg m^{-3}
(b) $h_c = 3.5(U/D)^{0.5}$ (Wm^{-2}deg^{-1}) See Constant C_6, **Table C-1.** D is wind travel distance across the body.

Effects of aging and physical condition in Man

As we have done elsewhere in closing a chapter or a section that deals mainly with physiological materials, we provide information about some of the effects of aging on human performance. In addition, we will present data exhibiting some of the effects of physical conditioning as they affect performance in younger and older human males. We include this information not so much because it is biometeorological in nature, but because it offers additional insights for

readers who may have cause to model the human energy balance in various contexts.

Bove (1983) characterizes the interactions among age, physical condition, and performance as follows:

> Although physical capacity is known to decline with age, it is unclear whether the loss of physical capacity is related to age or to the reduction in physical activity common among older individuals and to some extent caused by social factors that relegate physical activity and exercise to the younger population. There tends to be a deconditioning effect associated with age not because of age itself but because of the decline in physical activity as age progresses.

He provides support to the expected notion, that both age and condition are causal of the slow decline in performance, by citing studies of identical twins. The exercise performances of pairs at various ages — one twin being conditioned and one unconditioned — show that the decline can be reduced by remaining in good physical condition. Bouchard (1986) provides another kind of insight through other studies of identical twins, in which the pairs were of different age, gender, and prior physical training. One twin from each pair was trained for a particular physical task, and later testing showed that the twin receiving conditioning for that task showed essentially the same percent increase in performance over the other twin, irrespective of any other factor.

Medical evidence suggests that a slow, irreversible decrease occurs with aging in the flexibility of vascular walls, often termed "hardening of the arteries." This, in turn, results in a slow, irreversible decrease in the peripheral vascular conductance, represented in our model by ($\mathbf{h_b}$). These changes in flexibility are likely to be causally related to the normal increase with aging in blood pressure, which can be mitigated with a program of endurance exercise. It is also quite possible that these changes in ($\mathbf{h_b}$) are causally related to the decreasing tolerance of thermal discomfort in the elderly.

Finally, we offer quantitative information regarding these effects in **Table 15-5** and **Fig. 15-16**. **Table 15-5** provides data regarding maximum cardiovascular performance in human males for several classes of physical fitness. **Fig. 15-16** exhibits effects not only of age but also of metabolic work rate in human males for several measures of cardiopulmonary performance.

Concluding remarks

As regards the management of heat energy, and the effects of temperature and moisture on rates of development, there are strong, but often overlooked connections between plant ecology and animal ecology. It is clear that both plants and animals are linked to the atmospheric environment through direct, indirect, short-term, and long-term effects. While plants may not be said to exhibit movement

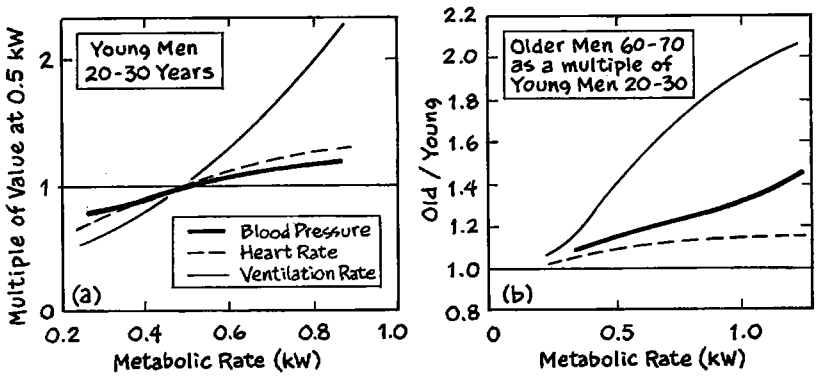

Fig. 15-16 The percent change in cardiopulmonary performance with age in human males depends on both the metabolic work rate and on the measure of performance. After Makrides *et al.* (1986).

in search of a preferendum, it is worth noting the similarity of postural thermoregulation in animals and the wilting and heliotropic responses of plants. Voluntary or involuntary, they all control the area factors; thus, they play a major role in the energy balances of the organisms involved. While plants do not have a response analogous to an animal's ingestive controls, it is reasonable to suggest that there is an analogy between an animal's architectural behavior and a plant's morphological adaptations.

At this point, the reader will no doubt see clearly that the physical principles involved in the management of heat energy by organisms,

TABLE 15-5 RATES OF DECREASE WITH AGE IN CARDIOVASCULAR PERFORMANCE OBSERVED IN ADULT MALE HUMAN BEINGS

Performance	Type of subject	Reduction, age 30 to 60		Source
		Amount	Percent	
Maximum rate of oxygen uptake[a]	Normal, healthy	41-29	32	Saltin (1986)
	Obese, untrained	38-28	26	Thompson and Dorsey (1986)
	Lean, untrained	44-33	25	Thompson and Dorsey (1986)
	Master athlete	66-51	23	Thompson and Dorsey (1986)
	Master athlete	78-54	31	Saltin (1986)
Efficiency of oxygen uptake[b]	Sedentary	22-17	23	Saltin (1986)
	Master athlete	40-32	20	Saltin (1986)
Supine arterial oxygen pressure	Athlete		11	Jones (1986)

NOTES:
(a) The rate of oxygen uptake is expressed in (ml $kg^{-1}min^{-1}$), as in the original reference. The reader is referred to **Appendix B** for the conversion: 1 ml $kg^{-1}min^{-1}$ = 0.338 W kg^{-1}.
(b) The efficiency of oxygen uptake is expressed in (ml $kg^{-1}min^{-1}$heart $beat^{-1}$), as in the original reference.

especially thermoregulation, cross all boundaries among plants, small vertebrates, insects, large vertebrates, Man himself, and Man's built environment. These same principles, of course, underlie the adaptations that together constitute Man's most powerful controls — clothing and architecture — as will become apparent in the next two chapters. It is increasingly becoming necessary for professionals from many fields — including scientists, planners, and designers — to be thoroughly familiar with these principles, and with the fact that the principles apply to so many facets of the study and application of ecology. At a time, such as the present, when society needs an increasingly comprehensive synthesis of knowledge about the principles of environmental science, delay in the achivement of that thorough familiarity can only hinder development of that synthesis. It will be one of our primary goals, as we move in the last two chapters to matters that relate exclusively to Man, to make clear the ways in which the same physical principles appear in many guises in our own management of heat energy.

Notes

(1) Data and analyses on which we have based our discussion of the Yellowstone elk herd are available in various casual publications from P.E. Farnes, Snowcap Hydrology, P.O. Box 691, Bozeman, Montana 59715, U.S.A. In particular, the data forming the basis for **Fig. 15-1** are found in a report dated 11 September 1993.

(2) The discussion of the climatology of respiratory afflictions and resorts will be reinforced by an examination of the Proceedings of the first three International Biometeorological Congresses organized by the International Society of Biometeorology and Bioclimatology, the third of which was published by Pergamon Press in 1967; and pages D4-D5 of "Report on Climate, Tourism, and Human Health," Publication WMO/TD-No. 682, World Meteorological Organization, Geneva, May 1995.

(3) Using a sample of experimental data from several sources, Campbell *et al.* (1980) suggested that the the effect of wind on the thermal resistance of animal coats and human clothing, (**r(U)**), is best represented by a function of the form $[r(U)]^{-1} = H(U) = A + B(U^n)$, where **H(U)** is the conductance of the coat, (**U**) is the speed of the air motion, (A) and (B) are experimental constants, and the exponent, (**n**), has a value close to unity. They contend that the model represents the data better than another form often used: $r(U) = [H(U)]^{-1} = C - D(U)^{0.5}$, where (C) and (D) are other experimental constants. Further, Campbell *et al.* point out that the value $n = 0.5$ seems to them "arbitrary and has not been critically tested." A still greater problem with the second form is that it predicts positive values of r(U) only for winds speeds less than $(A/B)^2$.

(4) Among many places in the literature, the graph is given on page 210 of Oke (1987), with units of resistance, (**r**), in $\{\text{sec m}^{-1}\}$, and on page 409 of Gates (1980), with units of insulation, (**I**), in $\{\text{m}^2 \text{ sec deg J}^{-1}\}$. Essentially the same information can be found on page 442 of Rosenberg *et al.* (1983). We consider the matter of different physical units for these data in **Box 15-2**.

(5) As a sample of many expressions for the dependence of the sweat rate (**SR**), on the core temperature, ($\mathbf{T_c}$), we offer these two. First, the graph on page 592 of Eckert *et al.* (1988) may be expressed by:

$$SR = 0.02 \qquad T \leq 36.85\,^{\circ}C.$$

$$SR = 0.0163 \text{ s } 0.949(T_{op}\text{-}36.85) - 0.121(T_{op}\text{-}36.85)^2 \qquad T > 36.85\,^{\circ}C,$$

where $\{\mathbf{SR}\}$ = (kW). Second, the graph for "Man" on page 439 of Rosenberg *et al.* (1983) may be expressed by either

$$(SR/M) = 8.88 - 0.633\ (T_{op}) + 0.0117\ (T_{op})^2, \text{ or}$$

$$\ln (SR/M) = -6.13 + 0.174\ (T_{op})$$

where (SR/M) is the evaporative heat loss as a multiple of metabolic heat loss. We note in passing that a third model for the evaporative heat loss of an exercising human being, used by Young (1979), includes a sweat term that is driven solely by the difference in vapor pressures between the skin and the ambient air — as from a fully wetted inanimate surface — without regard for experimental observations of the sweat rate.

(6) There are two reasons for the smaller range of values for sweat rates in **Table 15-2**, Set B, as compared with Set A. The first is the fact that the experimental arrangements for calorimetry in the case of Set B did not permit as full a range of activity by the human subject. The second is that the rates were given as volume flows in Set A, and we assumed — see note (c) in **Table 15-2** — that all sweat was being evaporated in converting the flow rate to energy units.

(7) In this regard, Lee (1968) presented the results in **Fig. 15-6** and gave credit to H.S. Belding and T.F. Hatch for the introduction in 1955 of the concept of relative strain.

(8) The results of Wyndham *et al.* and of Sargent *et al.* are reported in Givoni (1969, page 34). Sargent's results are confirmed elsewhere (Sargent, 1967), and he showed that each individual exhibited a distinct, personal, "signature-like" relationship of (**SR**) to time during prolonged exercise. The values of (**SR**) for an individual changed from one exercise period to the next — each person underwent six periods — but the basic pattern was always the same for each person. Sargent concluded that these patterns are genetically based. Moreover, observations of the same subjects revealed that, typically, their rectal temperature

rose 0.5 °C hr^{-1} during the first two hours, from 36 to 37 °C, followed by an increase at a constant rate of about 0.2 °C hr^{-1}, to 37.8 °C after 6 hours.

(9) Early and rudimentary experiments and mathematical modeling were reported in the efforts of Siple and Passel (1945) to quantify the effects of wind chill, and of Buettner (1951) to develop a mathematical basis for interpreting experimental observations made by the German military establishment during World War II. Although this work preceded that at Pierce Laboratory (for example, Gagge (1966)), the extensions of coordinated experiments and modeling by Lee and Henschel (Lee (1968)) may fairly be judged to be the foundation of the kinds of modeling studies we deal with in this book. The efforts of Lee and Henschel were later directed, in their work for the United States Public Health Service, toward understanding the tolerance of hyperthermal industrial environments by workers as a basis for regulations concerning occupational health in the workplace.

(10) In the same spirit as our other attempts to include an historical dimension to these two Volumes, we want to include this note, concerning a major academic program, during the 1960s, to train scientists for careers in biometeorology. Stanley Curtis and D.M. Driscoll are among the graduates of this program to whom we refer in this Volume. All doctoral candidates, the students who participated in this "traveling scholar program," were required to study in at least two universities of the Big Ten System, working with the expert faculty members, on their home campuses, who were also participants in the program. If they were primarily biologists, the students took training in meteorology, and in a major biological field if they were primarily meteorologists. The so-called C.I.C. Biometeorology Program was funded by the U.S. Public Health Service and the National Science Foundation, and it was administered by the Committee on Institutional Cooperation of the Council of Ten and the University of Chicago. (For example, see F. Sargent, II, 1965).

(11) We defined (Δ) as a withdrawal of body heat from the core. If, alternatively, we withdraw heat from the body itself rather than from the core, the partitioning of energy streams has (Δ) passing from Surface S to Surface X rather than from the core to Surface X. Defining the alternate conductance parameter for a large animal by $[1/\Sigma H_e + 1/H_f] = (1/K^{**})$, rearrangement yields the following alternative calculating model for large animals:

$$\Delta = K^{**}(T_c - T_{OP} - a_s A' S'/\Sigma H_c) - [1 + (K^{**}/H_b)] (M - LE)$$

which is an analog for **Eq.(15-5b)** and for which $\Delta = 0$ is the condition of thermal equilibrium.

(12) Laboratory results due to Herrington (1954, Figure 3), using human subjects in a controlled environment, exhibit the same

quasi-hyperbolic response produced by our model. Because he used a response variable roughly equivalent to our ($\mathbf{H_b}$) rather than ($\mathbf{k_b}$), Herrington's results and ours do not agree numerically. To make the results comparable, we have normalized them in the figure so that both have essentially the same maximum value on each coordinate.

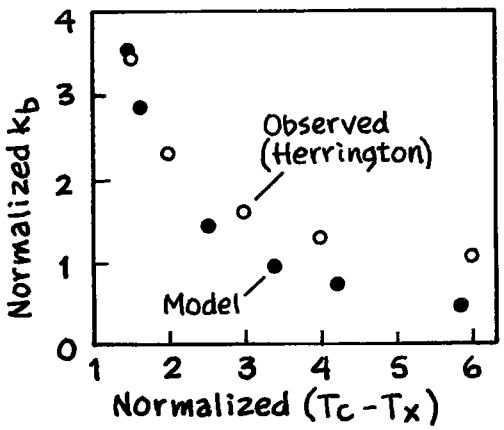

In addition to the rectangular hyperbola as a one-parameter approximation for the response of ($\mathbf{k_b}$) to (T_c - T_x), we considered also the two-parameter Michaelis-Menten function of **Eq.(B10-1a)**: $k_b = [(k_b)_{min}] \times [(K/\Delta T)+1]$. We applied these two functions to both our own model results and to the experimental results of Herrington. Our conclusion is that neither function is better than the other except that the former has only one parameter value. The "degree of fit" is suggested by the hyperbola displayed in **Fig. B15-2**.

(13) The quotation is from *Weather and Life* (Lowry, 1969, page 223) and the reference is to J.E. Heath, *Science*, November 6, 1964, page 784.

(14) James E. Heath, personal communication, May 1995.

(15) According to Landsberg (1969, page 41), A "person sitting quietly in a room with 21°C temperature, a draft of less than 3 meters per minute, and a relative humidity of 50 per cent" would be "in a state of comfort" wearing "an ordinary business suit" of insulative value 1 CLO while generating metabolic heat at the basal rate of 1 MET. Numerically, 1 CLO is 1.7 $\{m^2$ hr °C $kcal^{-1}\}$ and 1 MET is 50 $\{kcal\ m^{-2}\ hr^{-1}\}$.

(16) Withers (1992), page 129.

(17) David Gates and his students published a spate of fascinating papers on various aspects of the subject of convective phenomena associated with complex shapes of living plants and animals. For

example, concerning the use of cast metal models of plant materials, see Tibbals *et al* (1964), and concerning models of animal materials, see Bartlett and Gates (1967). Concerning the use of Schlieren photography, see Gates and Benedict (1963).

(18) For example, see Kelley *et al.* (1973), who measured swine with lines drawn parallel to the floor. They include additonal comments about how to make an estimate for the head and appendages, and they present technical details of the photogrammetric method. The following figure includes their results: a comparison of area estimates from their direct method (36 measurements on 8 animals), the photogrammetric method, and the use of an allometric relationship developed in the 1920s by Brody.

Kelley *et al.* explain that at least part of the difference between their results with direct measurement and those obtained with Brody's equation is due to the difference in shapes of commercially bred swine between the 1920s and the 1970s. The results in the figure do not seem to bear out the claims of "high precision and accuracy" made by one of Kelley's co-authors for his photogrammetric method.

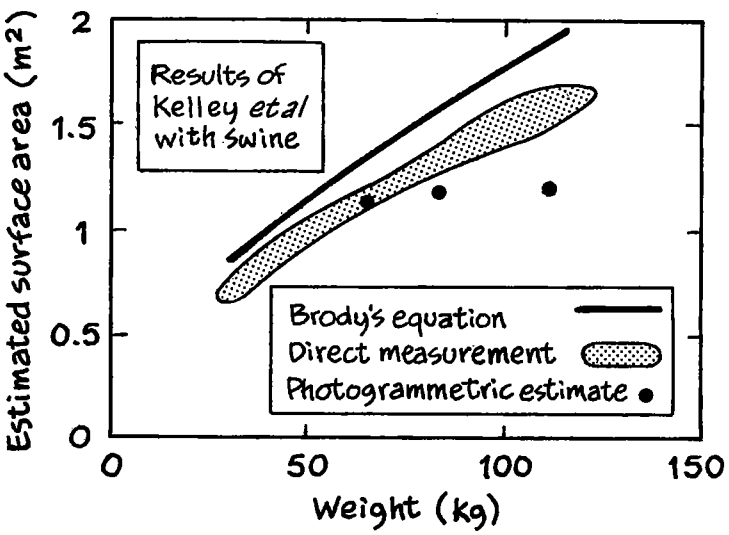

(19) Regarding the general structure of a boundary layer, see **Chapter 7, Volume 1**. Monteith (1973, page 114) mentions the use of a hot-wire anemometer and of Schlieren photography. Gates and Benedict (1963) describe the use of a thermocouple in conjunction with Schlieren photography.

(20) See Lee and Vaughan (1964), Lowry (1969, page 247), Landsberg (1972, page 31), and Munn (1970, page 198).

BOX 15-1 CALCULATIONS USING A MODEL FOR THE ENERGY BALANCE OF A LARGE ANIMAL

In this Box we will make use of the model for the energy balance of a large animal developed in **Chapter 15** in order to explore several relationships and concepts that arise in the study of animal thermoregulation, especially in Man. We begin by examining the nature of the relationship between the changing thermal environment and the body's "first line of defense" against thermal imbalance: its vasomotor responses, as quantified here by the body's thermal conductance, ($\mathbf{h_b}$), or its thermal conductivity, ($\mathbf{k_b}$). The two are related by the expression $(h_b) = (k_b)/(d_b)$, where ($\mathbf{d_b}$) is the length of the flow path for heat from the core to the skin surface — the "thickness" of the body shell.

By expanding the conductances — $[H_b = Ah_b]$ for the body and $[H_f = Ah_f]$ for the coat — and then rearranging **Eq.(15-4a)** we obtain

$$(T_c - T_x)\,(k_b) = [d_b + (k_b/k_f)d_f]\,(M + \Delta\text{-LE})\,(A)^{-1} \qquad \text{(B15-1)}$$

which relates the difference $(T_c - T_x)$ to ($\mathbf{k_b}$) directly. The difference is a measure of the thermal environment, while ($\mathbf{k_b}$) is a measure of the status of the vasomotor response. In thermal balance, with $\Delta = 0$, all the terms on the right side of **Eq.(B15-1)** are constant except the ratio, (k_b/k_f). The ratio is small when the animal being modeled is hairless or unclothed, and the right side of the equation is numerically nearly constant, so that the relationship expressed by **Eq.(B15-1)** is quasi-hyperbolic, as discussed also in connection with **Eq.(15-1)**.

In using the model, we set values for all parameters, and then obtained the value for ($\mathbf{k_b}$) that produced the condition $\Delta = 0$. The results are shown in **Fig. B15-1**, which verifies the observation that the relationship is quasi-hyperbolic. As further verification, we invite comparison of these computational results with the experimental results due to Herrington[12].

We wish to emphasize two other results from **Fig. B15-1**. The first is in **Fig. B15-1a**, which exhibits the fact that the response curve is the same for all environments modelled[H] as long as the animal itself is the same. The second result is in **Fig. B15-1b**, which shows that the response curve changes when the animal itself changes, in particular when the value of (**M**) changes to represent different levels of animal activity.

In **Fig. B15-2** we exhibit results related to the effects, on the quasi-hyperbolic relationship, of other, non-metabolic kinds of change in the animal: the body proportions and the thickness of the coat. Included for comparison[12] is the hyperbola $(k_b)(T_c - T_x) = 13$. Clearly, the relationships are quasi-hyperbolic; and, for the particular animals modeled, the effects of a change in body shape are about half as large as the effects of adding a coat, as may be judged by departures from a reference relationship: the animal with Shape A and no coat.

In **Fig. 15-6a** we considered observed values of the human sweat rate, (**SR**), as functions of the skin temperature, ($\mathbf{T_{sk}}$), and of the working metabolic rate, (**M**). Results obtained with the model for the energy balance of a large animal confirm the general form of the observed relationship, as shown in **Fig. B15-3**. The model permits us to understand something that the observations did not: that the relationship does not depend on the particulars of the thermal environment. In the calcu-

(H) In **Fig. B15-1** the environments differ in their relationships among ($\mathbf{T_a}$), ($\mathbf{T_r}$), and ($\mathbf{T_g}$); and in the value of ($\mathbf{S_d}$) and the relationship between ($\mathbf{S_d}$) and ($\mathbf{S_n}$).

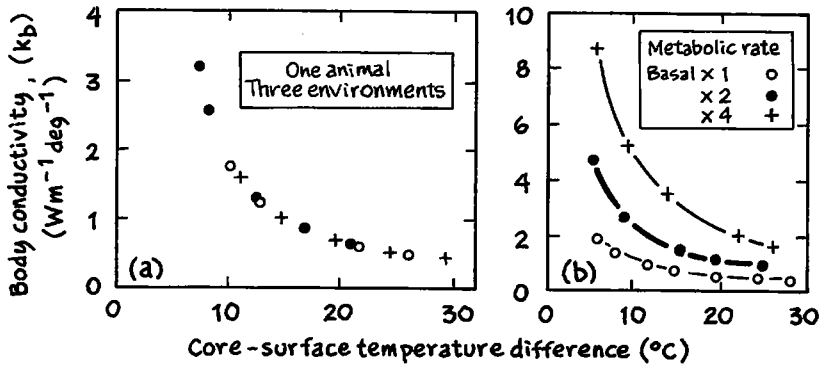

Fig. B15-1 Use of the model for the energy balance of a biped verifies laboratory observations that the functional relationship between (T_c-T_x) and (k_b) is quasi-hyperbolic. The model provides the additional information that **(a)** the functional relationship does not depend on the particular thermal environment; whereas **(b)** the functional relationship does depend on the values of system variables, in particular the metabolic work rate, (M).

The Animal		The environment	
Size (m): Diameter / Length	0.5 / 2.0	Direct shortwave flux, S_d (kW/m^2)	0.4, 0.7
Core temperature, T_c (°C)	38	Diffuse shortwave flux, S_n (kW/m^2)	0.1, 0.15(S_d)
Metabolic rate: multiples of M_b (W)	1,2,4 See Note(a)	Air temperature, T_a (°C)	Various
Body conductivity, k_b ($Wm^{-1}deg^{-1}$)	Various	Sky temperature, T_r (°C)	T_a, $T_a \pm 15$
Core-surface path, d_b (m)	0.3(D)	Ground temperature, T_g (°C)	T_a, $T_a \pm 15$
Coat conductance, h_f ($Wm^{-2}deg^{-1}$)	Various	Wind speed, U (m/sec) See Note(b)	0.5, 5
Ground conductance, h_g ($Wm^{-2}deg^{-1}$)	38	Solar zenith angle, Z	40
Coat shortwave absorptivity, a	0.7		
Latent heat loss rate, LE (Wm^{-2})	0.1(M)		

Notes:
(a) $M_b = 504.4\ (PD^3)^{0.75}$ (Watts) Use **Eq.(B13-4a)** with a sphere of density $10^3 kg\ m^{-3}$
(b) $h_c = 3.5(U/D)^{0.5}$ ($Wm^{-2}deg^{-1}$) See Constant C_6, **Table A-1**.

lations resulting in **Fig. B15-3**, we set values for all parameters and then obtained the value for (LE/M) that produced the condition $\Delta = 0$.

In discussion of **Fig. 15-7** we presented the concept of relative strain, (**RS**), defined by the relationship $RS = (SR_{req})/(SR_{max})$. We have used the model of the energy balance of a large animal to produce the results in **Fig. B15-4**, where lines of (RS) = 0.5 and 1.0 are plotted on coordinates of operative temperature and relative humidity. In our calculations $(SR_{req}) = \Delta$, which we obtain using **Eq.(15-5b)**. The formulation of (**SR_{max}**) is less direct. Recall that (**SR_{max}**) is the maximum rate of sweating possible under the ambient environmental conditions, and that (**SR_{max*}**) is the maximum rate of delivery that is physiologically and anatomically possible. Thus, $(SR_{max}) \leq (SR_{max*})$. Furthermore, Lee (1968) formulated (**SR_{max}**) so that it included the evaporative cooling from both breathing and sweating. Accordingly, we modeled (**SR_{max}**) as

$$(SR_{max}) = 100\ [e_{s(sk)} - R\ e_{s(op)}] + 20\ [e_{s(c)} - R\ e_{s(op)}]$$

where the symbols are defined in connection with **Eq.(15-3)**. In using the model, we set values for all parameters and then obtained the value of (**R**) that made (Δ/SR_{max}) equal a chosen value of (**RS**) — such as 1.0 — under the additional constraint that $(SR_{max}) \leq (SR_{max*})$ when we specified a value for (**SR_{max*}**). Lee's results in **Fig. 15-7** permit us to understand how the relative strain changes with changes in the physiological variable (**SR_{max*}**), and **Fig. B15-4** makes clear how it responds

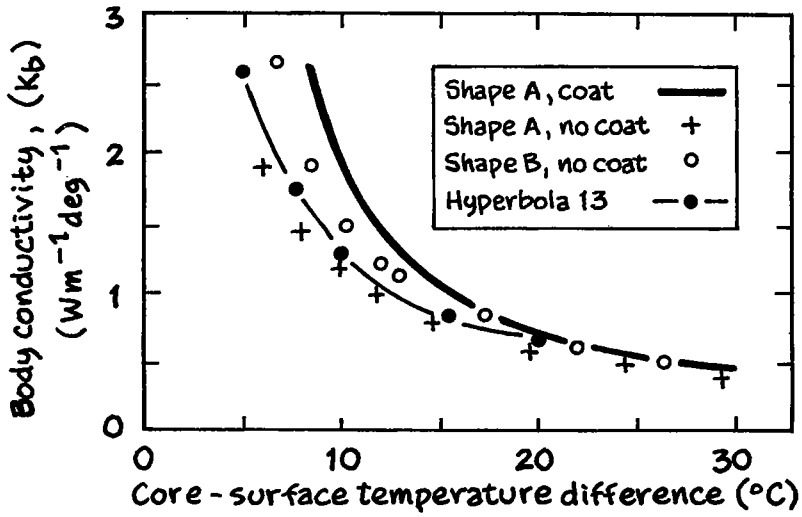

Fig. B15-2 Use of the model for the energy balance of a biped permits us to examine the effects of posture and of an animal coat on the quasi-hyperbolic functional relationship between (T_c-T_x) and ($\mathbf{k_b}$). The dimensions of the models with Shape A and Shape B appear in the following table, as does information on the coat. A rectangular hyperbola is exhibited for comparison.

The Animal		The environment	
Size (m): Diameter / Length	A=0.5/1; B=0.5/2	Direct shortwave flux, S_d (kW/m^2)	0.4
Core temperature, T_c (°C)	38	Diffuse shortwave flux, S_n (kW/m^2)	0.1(S_d)
Metabolic rate: multiples of M_b (W)	1 See Note(a)	Air temperature, T_a (°C)	Various
Body conductivity, k_b (Wm^{-1}deg^{-1})	3	Sky temperature, T_r (°C)	T_a-5
Core-surface path, d_b (m)	0.3(D)	Ground temperature, T_g (°C)	Not used
Coat conductance, h_f (Wm^{-2}deg^{-1})	1, 100 (h_b)	Wind speed, U (m/sec) See Note(b)	0.55
Coat shortwave absorptivity, a	0.7	Solar zenith angle, Z	40
Latent heat loss rate, LE (Wm^{-2})	0.1(M)		

Notes:
(a) M_b = 504.4 (PD^3)$^{0.75}$ (Watts) Use **Eq.(B13-4a)** with a sphere of density 10^3kg m^{-3}
(b) h_c = 3.5(U/D)$^{0.5}$ (Wm^{-2}deg^{-1}) See Constant C_6, **Table C-1.**

to changes in the environmental variable ($\mathbf{S_d}$). Clearly, increasing the shortwave radiant heat load decreases the range of tolerable environments for a given value of (**RS**).

Now we will examine briefly the hypothesis that human beings who are native to near-polar regions have evolved a "stocky" body shape more conservative of body heat in a cold climate than a "lanky" body shape. We will do this more to illustrate the utility of a relatively simple model of the energy balance of a large animal than to arrive at definitive results. In the model, the information on body shape is contained in the diameter, (**D**), in combination with the height, (**PD**), of the cylinder. In **Fig. B15-5** we have estimated the relative thermal imbalance, (Δ/**M**), as a function of body shape for two extremes: the sub-polar cold (C) season and the sub-tropical hot (H) season. As noted, the body shape is specified by (**D**) and by (**P**), and the subject has been modeled as being unclothed in order to exaggerate any relevant differences in (Δ/**M**). The "season" has been represented by a boreal night and by that hour on a subtropical day when the shortwave heat load is largest.

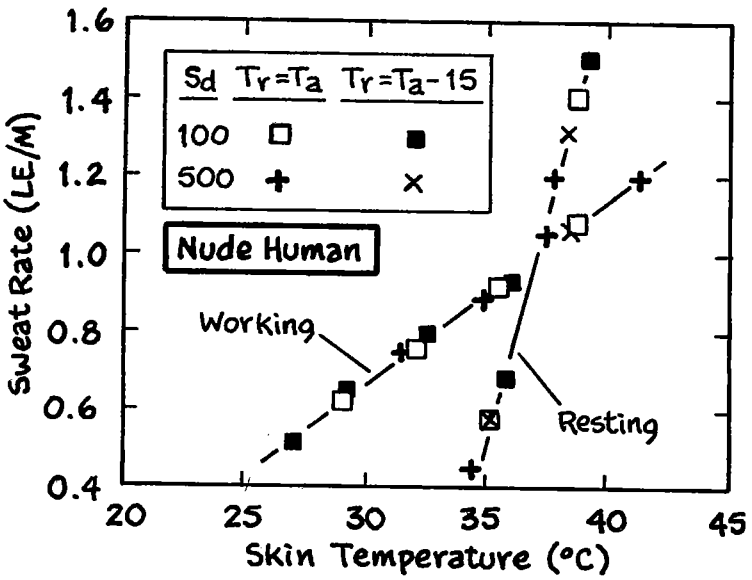

Fig. B15-3 The model of the energy balance of a large animal correctly predicts the general form of the relationship of the human sweat rate to the skin temperature, (T_{sk}), and the working metabolic rate, (**M**). Compare these predictions with the observed relationship exhibited in **Fig. 15-6a**.

The Animal		The environment	
Size (m): Diameter / Length	0.5 / 2.0	Direct shortwave flux, S_d (kW/m²)	0.1, 0.5
Core temperature, T_c (°C)	37	Diffuse shortwave flux, S_n (kW/m²)	0.1(S_d)
Metabolic rate: multiples of M_b (W)	1, 5 See Note(a)	Air temperature, T_a (°C)	Various
Body conductivity, k_b ($Wm^{-1}deg^{-1}$)	3	Sky temperature, T_r (°C)	T_a, T_a-15
Core-surface path, d_b (m)	0.3(D)	Ground temperature, T_g (°C)	Not used
Coat conductance, h_f ($Wm^{-2}deg^{-1}$)	$10^4(h_b)$	Wind speed, U (m/sec) See Note(b)	1
Coat shortwave absorptivity, a	0.7	Solar zenith angle, Z	30
Latent heat loss rate, LE (Wm^{-2})	0.1(M)		

Notes:
(a) $M_b = 504.4\ (PD^3)^{0.75}$ (Watts) Use **Eq.(B13-4a)** with a sphere of density $10^3 kg\ m^{-3}$
(b) $h_c = 3.5(U/D)^{0.5}$ ($Wm^{-2}deg^{-1}$) See Constant C_6, **Table C-1.**

The results shown in **Fig. B15-5** make clear that the effect on (**Δ/M**) is much less from differences in height, (**P**), than from differences in size, (**D**). At high latitudes, according to the model, a threefold increase in size — from D = 0.3 to 1.0 meter — reduces (**Δ/M**) by approximately one third — from 5 to 1.5; whereas, in the tropics body size and shape are essentially irrelevant to the problem of human thermoregulation. These results suggest that the largest seasonal strain is experienced by a small person in a cold climate, but that body size has at least some small degree of effect on (**Δ/M**) by changes in height. Extending these results to matters of nutrition and life style would be of interest, but they are beyond the scope of our inquiry.

An interesting anomaly has arisen in connection with the use of simple mathematical models to examine animal-environment interactions related to thermoregulation in ektotherms and endotherms. At the heart of the anomaly is what we call the "Classic Beer Can Experiment" conducted by Heath in 1964. Lowry put the anomaly in these words[13]:

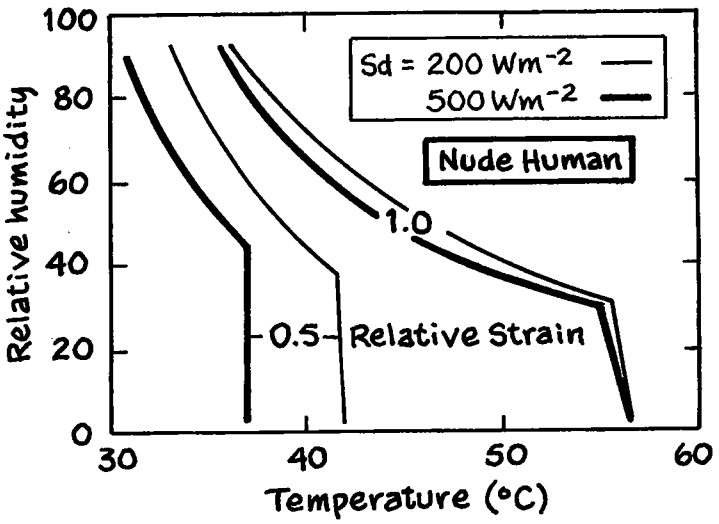

Fig. B15-4 Use of the model for the energy balance of a biped permits us to examine the effects of the shortwave radiant heat load on the relative strain of an erect human being, in the format of **Fig. 15-8**.

The Animal		The environment	
Size (m): Diameter / Length	0.3 / 1.8	Direct shortwave flux, S_d (kW/m²)	0.2, 0.5
Core temperature, T_c (°C)	37	Diffuse shortwave flux, S_n (kW/m²)	0.1(S_d)
Metabolic rate: multiples of M_b (W)	1 See Note(a)	Air temperature, T_a (°C)	Various
Body conductivity, k_b ($Wm^{-1}deg^{-1}$)	3	Sky temperature, T_r (°C)	Equal to T_a
Core-surface path, d_b (m)	0.3(D)	Ground temperature, T_g (°C)	Not used
Coat conductance, h_f ($Wm^{-2}deg^{-1}$)	0.1(h_b)	Wind speed, U (m/sec) See Note(b)	1
Coat shortwave absorptivity, a	0.7	Solar zenith angle, Z	
Latent heat loss rate, LE (Wm^{-2})	0.05(M)		
Maximum SR, (SR_{max*})(Wm^{-2})	500		

Notes:
(a) M_b = 504.4 $(PD^3)^{0.75}$ (Watts) Use **Eq.(B13-4a)** with a sphere of density 10^3kg m^{-3}
(b) h_c = 3.5$(U/D)^{0.5}$ ($Wm^{-2}deg^{-1}$) See Constant C_6, **Table C-1.**

The shape of the distribution curve [of the choices of water temperature made by the goldfish in **Fig. 13-11a**] — with a tailing off toward the lower temperatures — is intriguingly similar to frequency distributions of the body temperatures of reptiles measured in the field. The similarity may be coincidental, however, since, as Heath points out, the observed temperatures of the reptiles do not necessarily represent behaviorally regulated results. He reached this conclusion after obtaining a similar distribution by measuring temperatures of beer cans [that were wholly- and partially-filled with water] at randomly selected times on a sunny day. The temperatures he obtained are clearly just the equilibria of the inanimate systems, and the point is well made that analyses of field data should be approached with caution. The easy and tempting transfer from a true preferendum such as that in [the figure of the goldfish] to a similar interpretation for the field data Heath describes must be avoided.

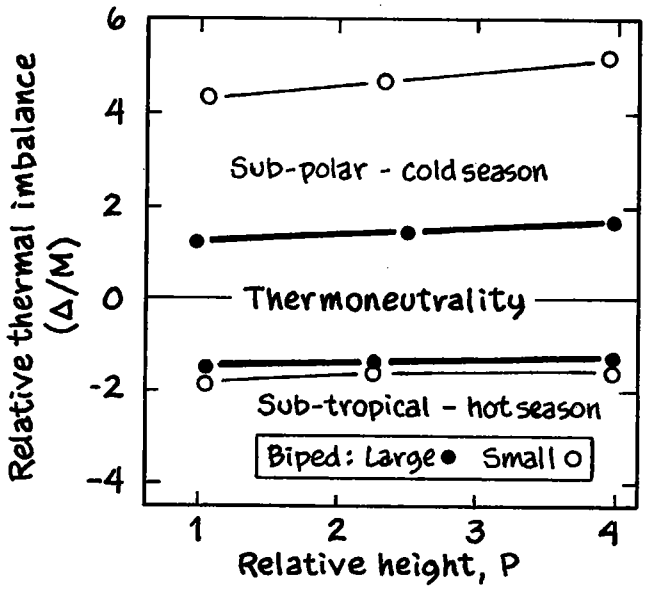

Fig. B15-5 Use of the model for the energy balance of a biped permits us to examine the effects of body shape, expressed in the relative height parameter, (**P**), on the relative thermal imbalance of an erect human being. In partiucular, we may conclude that body shape has only a minor effect on the conservation of body heat in climatically extreme environments.

The Animal		**The environment**	
Size (m): Diameter / Length	0.3 / 1.0	Direct shortwave flux, S_d (kW/m^2)	C=0, H=700
Core temperature, T_c (°C)	38	Diffuse shortwave flux, S_n (kW/m^2)	0.1(S_d)
Metabolic rate: multiples of M_b (W)	1 See Note(a)	Air temperature, T_a (°C)	C=-20, H=36
Body conductivity, k_b (Wm^{-1}deg^{-1})	3	Sky temperature, T_r (°C)	T_a-15
Core-surface path, d_b (m)	0.3(D)	Ground temperature, T_g (°C)	Not used
Coat conductance, h_f (Wm^{-2}deg^{-1})	10^4(h_b)	Wind speed, U (m/sec) See Note(b)	1
Coat shortwave absorptivity, a	0.7	Solar zenith angle, Z	C=90, H=41
Latent heat loss rate, LE (Wm^{-2})	0.1(M)		

Notes:
(a) $M_b = 504.4\ (PD^3)^{0.75}$ (Watts) Use **Eq.(B13-4a)** with a sphere of density 10^3kg m^{-3}
(b) $h_c = 3.5(U/D)^{0.5}$ (Wm^{-2}deg^{-1}) See Constant C_6, **Table C-1.**

Some years later, Withers (1992, page 140) exhibited a scatterplot of data pairs — collectively labelled "Metal can" — of "Air Temperature" *versus* "Body Temperature." We have reproduced that presentation as our **Fig. B15-6**. The only indication in Withers as to what these data represent or how his readers are to interpret them is the part of the figure caption reading "Also shown [for comparison with data on thermoconforming and thermoregulating lizards] is the relationship for an inanimate object (water-filled metal can)."

Elsewhere in the same textbook, Withers (1992, page 154) tabulated the data we have presented earlier, in a different context, in our **Fig. B14-16**. The data consist of a table of coefficients, (a) and (b), representing regression models, for a wide range of ektotherms and endotherms, in the form

Body temperature = a + b (Air temperature).

In Withers' long list of coefficients is an entry marked "water-filled metal can: passive." The data for the can are: a = 24.3; b = 0.30 — which plot near where the data for ektotherms and the data for endotherms meet in our **Fig. B14-16.** In that figure, the data for the inanimate metal can merge with the data for living animals, without appearing anomolous in any way.

Withers gives no basic information concerning the experiments that yielded the data on the metal cans, so we cannot compare those experiments with Heath's experiment. Withers' entries give no information about whether there was one or (as in Heath's experiment) more than one can; the size of the can or cans; whether the amount of water enclosed was held constant; whether the observations were made in the open or under controlled laboratory conditions; nor the nature of the observation schedule. Because it seems to us unlikely that an inanimate, water-filled, metal can is somehow intermediate between ektotherms and endotherms, we propose now to present what we consider to be the likely explanation of the data representing the metal cans.

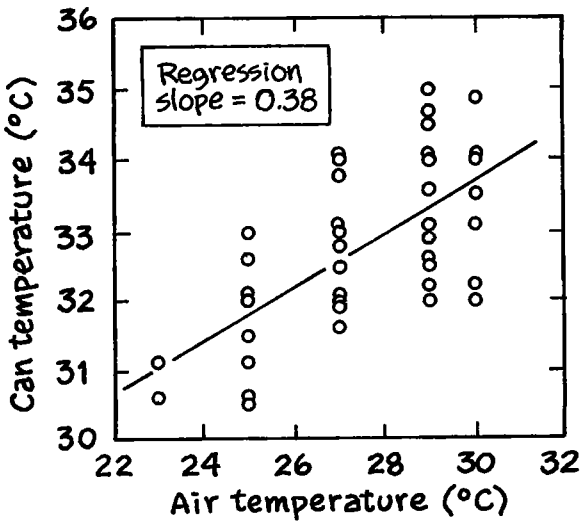

Fig. B15-6 Observations of air temperature and of water in a metal can are purported to demonstrate a principal concerning thermoregulation in thermoconforming and thermoregulating lizards and in inanimate objects. The array is adapted from Withers (1992, page 140) who, unfortunately, provides neither a statement of the principle nor information about how the observations were made.

We begin by asserting that the diurnal trace of the temperature in a water-filled can, with a non-negligible thermal time constant, will be a modified copy of the trace of air temperature, with a smaller amplitude and a time lag. The simultaneous sampling of these two traces on almost any time schedule will yield a plot of data pairs resembling that in **Fig. B15-6.** To demonstrate the basis for our assertion, we will use a simple sine wave as a basic calculating model for the diurnal trace of air temperature:

T_a = sin (A)

where (A) = (n-6)x(15 °) and (**n**) is the hour number beginning with zero at midnight. Thus, at hour 18, (T_a) = sin (12)x(15 °) = 0; it falls to a minimum of sin

(-6)x(15°) = -1 at midnight; to zero again at hour 6; and rises to a maximum of sin (6)x(15°) = 1 at noon. As the calculating model for the diurnal trace of the "can temperature" we will use:

$$T_c = \sin(B) = a\,[\sin(A - d)]$$

where (**a**) is the amplitude ratio of (T_c) relative to (T_a) — between 0 and +1 — and (**d**) is the time delay of (T_c) behind (T_a) — between 0 and 12.

When there is no time delay — when d = 0 — the pairs of simultaneously sampled temperatures will plot as a straight line, with slope equal to (**a**), on coordinates of $T_a = \sin(A)$ and $T_c = \sin(B)$, as in **Fig. B15-7a**. On the other hand, when d ≤ 0 and for any constant, non-zero value of (**a**), the pairs of simultaneously sampled temperatures will plot as a family of ellipses, one for each value of (**d**), as in **Fig. B15-7b**. As (**d**) increases from 0 to 12, the plots change from a straight line with slope equal to (**a**), through a sequence of ellipses, to a circle. Thus, **Fig. B15-7** separates the calculated results due to changes in (**a**) from those due to changes in (**d**).

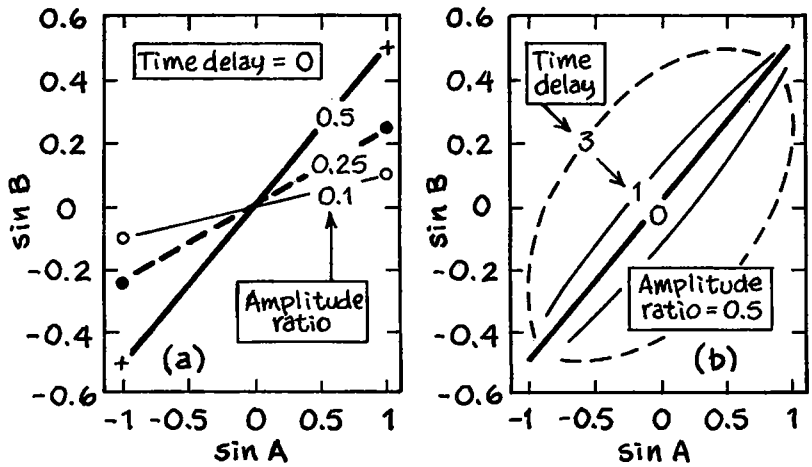

Fig. B15-7 **(a)** Loci of plots of air and can temperatures, with time delay (d) = 0 and amplitude ratio (a) = sin(B)/sin(A) = 0.1, 0.25, and 0.5. **(b)** Loci of plots of air and can temperatures, with (a) = sin(B)/sin(A) = 0.5 and time delay (d) = 0, 1, and 3.

In **Fig. B15-8a** we have plotted simulated hourly observations for an assortment of pairs of values for (**a**) and (**d**). Among these pairs, (**d**) and (**a**) are inversely proportional, as would be the case for a sample of inanimate metal cans with a range of thermal time constants. Such an increase in the time constant could be due to some combination of three reasons: (i) the can is larger, (ii) the can contains more water, or (iii) the environment is increasingly cloudy. In **Fig. B15-8a** we have used two symbols to separate daylight hours from nighttime hours. In **Fig. B15-8b** we have removed the data points representing nighttime and added a line with slope equal to that of the regression line in **Fig. B15-6**. The result bears a strong resemblance to **Fig. B15-6**, clearly suggesting that the data in that figure probably came from a physical system much like the one we have used in our simulation, rather than as implied by Withers.

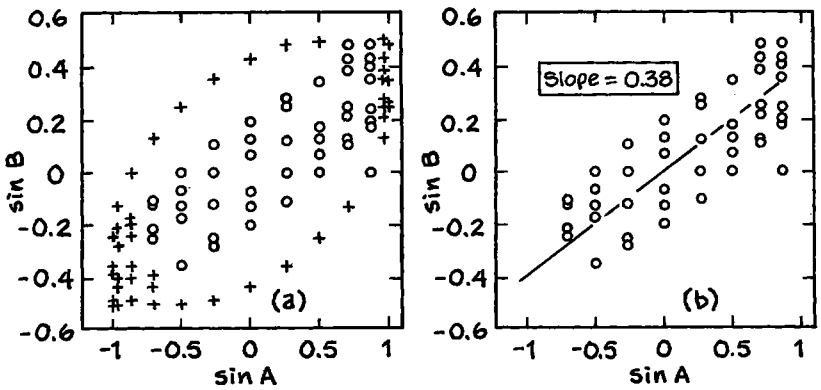

Fig. B15-8 Simulated hourly data pairs of air and can temperatures, obtained by using assorted pairs of values for the amplitude ratio, (**a**), and the time delay, (**d**), in conjunction with the models $T_a = \sin(A)$ and $T_c = \sin(B) = a[\sin(A - d)]$. The pairs shown by small crosses in (**a**), representing nighttime hours, have been removed in (**b**), where a regression line has been added, with the same slope as that shown in **Fig. B15-6**.

Our closing comment pertains to the significance of a coefficient of linear correlation, (**r**), as in **Fig. B15-6**. According to the theory of linear, least squares regression, even a set of data pairs that fits perfectly on a straight line will have an insignificant value of (**r**) if that line is nearly horizontal or vertical. If the line is horizontal, for example, the plot depicts the fact that the data on the abscissa contain no information about those on the ordinate. In our system of two sine waves, the slope of the axis of an ellipse approaches zero as the amplitude ratio, (**a**), approaches zero; that is, as the effective thermal time constant increases. Examples showing this, for the case when $d = 0$, are in **Fig. B15-7a**. It is an interesting fact that, for a given value of the amplitude ratio, (**a**), the slope of the linear regression model calculated for the ellipse also approaches zero as the time delay, (**d**) — that is, the effective thermal time constant — increases. We have illustrated these comments in **Fig. B15-9**. In **Fig. B15-9a** an ellipse with an amplitude ratio of $a = 0.5$ and a time delay of $d = 4$ has a slope of $+0.5$ for the major axis, but it has a slope of $+0.27$ for the linear regression model. **Fig. B15-9b** presents all cases of this difference in slopes, and the large cross locates the conditions depicted in **Fig. B15-9a**: $a = 0.5$, $d = 4$.

While it may be interesting that the data sets for water-filled cans in Withers' presentations appear to represent a true *transition* from the behavior of thermoconforming animals to that of thermoregulating animals; we conclude that the statistics and the appearance of transition are irrelevant to the matter of an animal's thermal economy. The slope and the appearance of transition are as likely to be artifacts of the physical environment in which the temperatures of the water in the experimental cans were measured, and of the observation schedule, as of anything about the cans themselves. In the same manner, the shape of a distribution curve of the body temperatures of reptiles measured in the field is as likely to be an artifact of their physical environment and of the observation schedule as of anything about the animals themselves. In the case of a controlled experiment with either cans or ektotherms, any correlation could be made statistically significant or insignificant

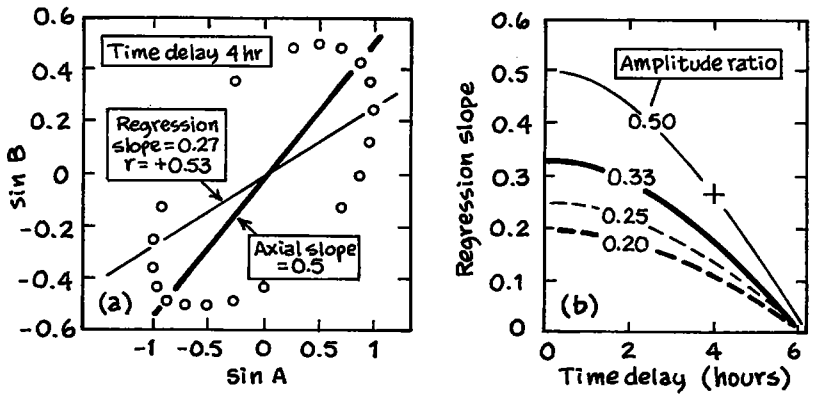

Fig. B15-9 (**a**) A plot of simulated hourly observations of air and can temperature pairs has a slope of +0.5 when the amplitude ratio is 0.5; but the same plot has a regression model with slope +0.27. (**b**) A summary of the relationships among the amplitude ratio, (**a**), the time delay, (**d**), and the slope of the associated linear regression model for several values of the amplitude ratio. The large cross locates the conditions depicted in panel (**a**).

by appropriate changes of the environment and the observation schedule of the experiment. Heath advises[14] that "a proper control for field observations of [these animals] would be (i) an appropriately-sized [inanimate] black body, (ii) an animal tethered in the sun so that behavioral methods are denied, or (iii) a freshly-killed specimen." We summarize these beer can experiments with the assertion that the results in Withers are merely fortuitous, not biophysically significant.

BOX 15-2 A NOTE ON RESISTANCE AND CONDUCTANCE

In **Chapter 4** of **Volume 1**, and again in **Appendix C** of this volume, we have introduced and used the notion of thermal resistance as approximately the inverse of thermal conductance. In this Box we consider several of the versions employed by various writers for these two concepts in the literature on animal biometeorology, especially human biometeorology. In particular we note some of the difficulties in interpretation of numerical values for these variables when authors use different physical units.

The module for the rate of transfer of sensible heat, (**H**), found in a study of an animal's energy balance usually takes one of the following forms:

$$H = (k/\Delta z)(\Delta T) = h(\Delta T) = (\varrho c/r)(\Delta T) = (\Delta T)/I \qquad \text{(B15-2)}$$

On **page 68** of **Volume 1** we suggested that these modules were either of the form [(Conductance)x(ΔT)] or of the form [(ΔT)/(Resistance)]. Elsewhere in both **Volumes 1** and **2** we have referred to the multipliers of (ΔT) as transfer coefficients. Clearly, the terminology in the literature is consistent in general, but careful inspection shows that it is often inconsistent in the details. For example, by one convention we should equate (Resistance) with ($r/\varrho c$) and, by another, with (**r**). This matter is partially untangled when we recall, as indicated in **Box 7-2**, that the property being transferred is not temperature, but the heat per unit mass of air at temperature (**T**), which is ($\varrho c_p T$). That being the case, it is (**r**) that is properly called (Resistance).

For another example — usually encountered in the literature of human medical biometeorology — the insulation, (**I**), is of the form we have prescribed for (Resistance), as in the last module of **Eq.(B15-2)**. The standard unit for (**I**) in human biometeorology is 1 CLO = 1.7 $\{m^2\ hr\ °C\ kcal^{-1}\}$[15]. By inspection we see that the units for (**I**) are the inverse of those for the transfer coefficient, (**h**). Before going on we wish, for reference later, to distinguish between the thermal conductance, (**h**) — with units of $\{W\ m^{-2}deg^{-1}\}$ — and the thermal conductivity, $k = h(\Delta z)$ — with units of $\{W\ m^{-1}deg^{-1}\}$. Furthermore, and regardless of the relative merits of the various formulations, the following identities are useful:

$$k = h\ (\Delta z) = (\Delta z)/I \text{ with units of } \{W\ m^{-1}\ deg^{-1}\} \qquad \text{(B15-3a)}$$

and

$$rk = (\varrho c)(\Delta z) \text{ with units of } \{W\ sec\ m^{-2}\ deg^{-1}\} \qquad \text{(B15-3b)}$$

We encountered — on a single page, and without comment by the author — a list of values for the resistances of various materials[16] tabulated in two columns: one with units of $\{sec\ cm^{-1}\}$ and the other with units of $\{CLO\ m^{-1}\}$. Our conversions of these numerical values to values in standard units for conductance and conductivity yielded values that were not in agreement with those we knew to be correct; for example, with those in **Table 4-2** of **Volume 1**. Because of those disagreements, we decided to prepare this Box. The following is an attempt to explain the reasons for the disagreements.

The units $\{sec\ cm^{-1}\}$ — the first column in the listing just cited — are those for (**r**), but they require, for conversion to other units, a knowledge of the associated value of (ϱc), and thus of the transfer medium — air, water, or some other material — used in the calculations of the tabulated values. While one may infer which medium was used for the calculations upon which the listings were based, it appears that those drawing up the list[16] almost certainly used the same value of (ϱc) for all entries in a list of materials that include both air and water as transfer media.

The units $\{CLO\ m^{-1}\}$ — the second column in the listing of resistances just cited — are the units for (1/k). The authors of that listing, however, specified alternate units of $\{m\ sec\ °C\ J^{-1}\}$ which are not strictly speaking those of $\{CLO\ m^{-1}\}$. With these comments we want to make the point that the presentation of units in a less-than-explicit manner, by some authors, makes it difficult for others to merge entries from several sources into a list such as the one given below in this Box.

Experimenters often obtain estimates of whole-body conductance, ($\mathbf{h_b}$) or its inverse, (**I**), by exposing the animal in a calorimeter, measuring the animal's rate of heat production, (**M**), its surface area, (**A**), and its rectal and surface temperatures, ($\mathbf{T_{re}}$) and ($\mathbf{T_s}$), and then calculating an estimated conductance according to:

$$h_b = M/A(T_{re} - T_s) \qquad \text{(B15-4)}$$

The estimates are then reported with the appropriate physical units of (energy)/(time)(area)(degrees), but usually without the experimenter giving consideration to its use in connection with any other animal. As a consequence, one is not always able to discern directly the size of the animal in order to estimate a value of $k = h(\Delta z)$ from the reported value of ($\mathbf{h_b}$). That is, the surface area of the animal is implicit in the reported value for ($\mathbf{h_b}$), which can present a problem when one wishes to compare numerical values for conductive parameters taken from various sources, as an aid in modeling generalized animals.

The following Table provides a list of values for thermal conductance, with units of {W $m^{-2}deg^{-1}$}, expressed as multiples of standard values for still water and still air. When the source for a particular value reported a conductance, (h_b), we have tabulated it in standard units. For a reported value of conductivity, (k_b), on the other hand, we have tabulated the value for a path length of $\Delta z = 1$ meter. We believe that reporting the conductive properties of various materials in this way — as multiples of standard conductances — permits the greatest flexibility in using this information to construct generalized mathematical models for the study of the energy balances of animals. In using the table to convert a value of (h_b) to a value of (k_b) for modeling across a range of animal sizes, one may assume an appropriate conductive path length, (Δz), for the size of the generalized model animal and then calculate the conductivity, (k_b), according to $k = h(\Delta z)$.

Material	Conductance as a multiple of the value for Still water	Still air	Reference
BUILDING MATERIALS			
Still air	0.033	1.0	Table 4-2, Volume 1
Wood (typical)	0.18	6.0	Mean of Table 4-2 and Withers (1992), Table 5-3
Dry soil	0.51	17.0	Mean of Table 4-2 and Withers (1992), Table 5-3
Still water	1.0	30.0	Table 4-2, Volume 1
Window glass	1.7	41.6	Withers (1992), Table 5-3
ANIMAL TISSUE			
Animal fat	0.27	8.1	Withers (1992), Table 5-3
Human tissue	0.73	21.9	Withers (1992), Table 5-3
Human skin, cool	0.86	25.7	Buettner (1951)
Human body, cool	3.7	110.	Herrington (1954)
Human skin, warm	6.6	199.	Buettner (1951)
Swine body, cold	10.8	324.	Curtis (1981), Table 4-1
Cow body, cold	11.4	343.	Curtis (1981), Table 4-1
Human body, warm	20.3	608.	Herrington (1954)
Sheep body, cold	23.0	690.	Curtis (1981), Table 4-1
Swine body, warm	30.6	919.	Curtis (1981), Table 4-1
Human finger, cool	31.7	952.	Ingram and Mount (1975) page 65
Cow body, warm	36.7	1102.	Curtis (1981), Table 4-1
Sheep body, warm	61.3	1838.	Curtis (1981), Table 4-1
Human finger, warm	87.3	2619.	Ingram and Mount (1975) page 65
ANIMAL INSULATION			
Fox fur	0.057	1.52	Mean of Withers (1992), Table 5-3, and Oke (1987), Table 6.3
Sheep wool	0.10	2.75	Mean of Withers (1992), Table 5-3, and Oke (1987), Table 6.3
Bird feathers, flat	0.103	3.1	Withers (1992), Table 5-3
Bird feathers, erect	0.25	7.6	Withers (1992), Table 5-3

Reference values for thermal conductance (W $m^{-2}deg^{-1}$): Still air = 0.021; still water = 0.63 (Source: **Table 4-2, Volume 1**).

The wide range of magnitudes for animal flesh in various forms and stages of vasomotor regulation serves mainly to emphasize (i) the uncertainties inherent in the experimental values and (ii) the fact that variable conductance (and resistance) constitutes a major means employed by larger endotherms to achieve thermoregulation, in contrast to the variable metabolic rates employed by smaller endotherms.

We close this Box by illustrating one use of the type of standardized data presented in this table, with calculation of values for ($\mathbf{k_b}$) that we used in the mathematical models of small endothermic animals in **Chapter 14**. There we used a path length of $\Delta z = 0.1$ meter for the human body to estimate ($\mathbf{k_b}$), using Herrington's values of ($\mathbf{h_b/h_{water}}$) from the table, as follows:

$$k_b = (h_b/h_{water})\ (h_{water})\ (\Delta z)$$

which for a cool animal body — capillaries constricted — is

$$k_b = (3.7)\ (0.63)\ (0.1) = 0.23\ \{W\ m^{-1}deg^{-1}\}$$

and for a warm animal body — capillaries dilated — is

$$k_b = (20.3)\ (0.63)\ (0.1) = 1.28\ \{W\ m^{-1}deg^{-1}\}.$$

Accordingly we used the range $[0.25 < k_b < 2]$ in our calculations for the Figures in **Chapter 14**.

BOX 15-3 EXPERIMENTAL TECHNIQUES USED IN QUANTITATIVE RESEARCH ON THE ENERGY BALANCE OF AN ANIMAL

In this Box we discuss, in very general terms, several techniques by means of which investigators have obtained estimates of the values of various parameters discussed in **Chapters 14, 15** and **16**. Our principal purpose is to enhance the reader's basic appreciation for the process of mimicking the energy balance of a living animal with either a physical or a mathematical model of that balance, rather than to examine the details of experimental techniques.

It is relatively simple, as we have done in following the work of many modelers, to mimick mathematically the various areas of a living animal by using a cylinder with diameter, (**D**), and height, (**PD**) — a "beer can" model. It is quite another matter, however, to estimate the true areas of variously shaped bodies, as one might wish to do when using a physical model. Accordingly, we offer brief descriptions of several techniques for doing this, some of which are among the most inventive ideas in the literature on the biometeorological energetics of organisms.

1) Estimation of the total surface area of an animal, A. By means of an electrolytic technique used by Gates[17], one may estimate the total area of a small animal with great accuracy. The method requires considerable technical skill, and it is not feasible if the animal is larger than, say, a rat. The method can also be used for plants and plant parts, such as small leaves or conifer branchlets. With a metal casting of the small animal (or plant materials) as one electrode, the electric current flowing to the other electrode is then a function of the total area, (**A**), for a given voltage, regardless of the complexity of the shape.

For larger animals, biometeorologists have used some form of either direct or photographic measurement to estimate the total area. For example, using a marking pen attached to a rigid structure located beside the standing animal, one may draw circumferential lines a constant distance apart on the surface, say 2 cm. The estimate of area for the body is obtained by measuring the total length of lines drawn

and multiplying by 2 cm. In addition, biometeorologists have used stereoscopic photographs in conjunction with standard cartographic methods for drawing contours and calculating surface areas of large animals[18].

2) Estimation of the surface area of an animal in contact with a substrate, A_c. Gates and his students estimated ($\mathbf{A_c}$) using the same electrolytic technique just mentioned. They smeared the "contact area" on the metal casting with an insulating grease; measured (A-A_c) in the electrolytic bath; and then subtracted that value from the value of (**A**) obtained previously. The same idea can be used, of course, by smearing the grease everywhere on the model except the contact area, thereby obtaining ($\mathbf{A_c}$) directly.

In a form of direct measurement, animal scientists studying larger species have often photographed animals, in any posture, from beneath a transparent floor of their enclosure. In such a photograph the area of contact is readily apparent, and can be estimated by ordinary planimetric methods.

3) Estimation of the shadow area of an animal, A_d. The estimation of a shadow area — the area on which direct shortwave radiation impinges — is inherently straightforward. A colimated light source and a surface containing a grid comprise the entire "instrumentation" required. The advantages of using a model of an animal are obvious, including the ability to specify the orientation of the animal with respect to the sun. There are several techniques for measuring the area of a shadow. In addition to the use of a planimeter, one may draw the outline of the shadow, cut out the paper or light cardboard on which the shadow fell, and compare the weight of the cutout shadow area with a known weight for a unit of area. Use of a flatbed scanner is often available as a technologically sophisticated addition to the list of methods.

Our experience with the basic method of casting a shadow on a grid has provided some interesting and useful results. We obtained, from each member of a class of 18 students, a set of observations: (i) the student's height, (**H**); (ii) the student's estimate — with the aid of a classmate — of the shadow area cast on a gridded, horizontal surface, ($\mathbf{A_{dh}}$), with the student's back to the sun; and (iii) the time of the observation, which permitted calculation of the solar zenith angle, (**Z**). These observations, together with a formula for the area of a cylinder cast on a surface normal to the solar beam, ($\mathbf{A_{dn}}$), enabled us to calculate, for each student, the diameter of a cylinder, (**D**), that would have cast the same area of shadow as the student cast. Knowing that $(A_{dn}/A_{dh}) = \cos Z$, and that, for the cylinder, $(A_{dn}) = D(H_n)$ and $(A_{dh}) = D(H_h)$, one may insert the student's values of (**H**) and (**Z**) in the formula and then vary the value of (**D**) until the value of the output $[(A_{dn})/\cos Z]$ is equal to the value of ($\mathbf{A_{dh}}$) observed by the student.

Statistics for the class yielded the results that, for the required diameter, (**D**), the mean and one standard deviation $= 0.3 \pm 0.03$(m), with $H = 1.73 \pm 0.08$(m), and essentially no correlation between the two. We note that D.H.K. Lee used $D = 0.3$ in his modeling of soldiers and industrial workers. The values of (**D**) would be smaller, of course, if the students had estimated ($\mathbf{A_{dh}}$) while facing at an oblique angle to the sun. Further, from estimates of ($\mathbf{A_{dh}}$) made by the students while they were squatting with their back to the sun, we obtained a sample of values for the ratio ($A_{dh,squat}/A_{dh,stand}$). The result for this ratio was that the mean and one standard deviation $= 0.79 \pm 0.07$.

4) Estimation of the area of an animal involved in longwave radiant and convective energy exchanges, A_e. The last of the four areas usually required for modeling is what the physicist-turned-biometeorologist, David Gates, has called the "extended area, ($\mathbf{A_e}$)." In essence, it is the total area reduced by the amount of area

hidden from direct, external view in the folds of the body and appendages. While it is deceptively simple in a beer can model — (A-A_c) — it is in actuality probably the most difficult of the four areas to estimate. A method for precise estimates of ($\mathbf{A_e}$) has been made available to us, again for very small animals, and again through the imagination of Gates. The procedure involves the pre-heating of a metal casting — characterized by mass (**m**), specific heat (**c**), and longwave emmissivity (ϵ) — followed by its suspension in a vacuum chamber. At a time when the temperature of the casting is ($\mathbf{T_c}$) and that of the chamber walls is ($\mathbf{T_w}$), the rate of radiant heat transfer from the casting to the walls — the only mode of heat transfer in the vacuum chamber — is

$$\epsilon_c \sigma (T_c^4 - T_w^4) \ (A_e) \qquad \text{(B15-5a)}$$

and the rate of cooling of the casting is

$$mc(dT_c/dt). \qquad \text{(B15-5b)}$$

Since the two expressions are equal to each other, we obtain

$$A_e = [mc(dT_c/dt)] \ / \ [\epsilon_c \sigma (T_c^4 - T_w^4)]. \qquad \text{(B15-5c)}$$

We are not aware of any means for estimating ($\mathbf{A_e}$) for large animals. Curtis (1981) and Lee (1968), for example, simply "finesse" the matter by including the area in an equation and then ignoring the means for evaluating it. Elsewhere Lee (1964, page 558) merges ($\mathbf{A_e}$) with ($\mathbf{h_c}$) for a soldier, and gives an all-purpose numerical value of $H_e = A_e h_c$ without explaning how he evaluated it. We suspect that most modelers use ($\mathbf{A_e}$) = (**A**) and accept the assumption, reasonably or not, that this approximation is within the margin of error for other terms in the energy balance.

In addition to the areas involved in an energy balance there are, of course, dynamical elements that require estimation for some purposes. Probably the most important of these dynamical elements are the dimensions of the microscale boundary layer surrounding the animal. We offer a short list of techniques for estimating them.

5) Estimation of physical dimensions of microscale boundary layers involved in convective energy exchanges. Early students of the energy balances of animals adapted several techniques from aeronautical and heat transfer engineering to gain an understanding of the physical dimensions of the microscale boundary layer surrounding a complex shape. We mention two kinds of technique. The first involves the use of a tiny probe to explore differences and gradients in some atmospheric property that serves as a tracer. A thermocouple or a thermistor serves as a probe to estimate temperature; whereas, a hot-wire anemometer permits the estimation of speed. With a generalized notion of how temperature and speed vary within a boundary layer, one can obtain a reasonably complete picture of the layer surrounding the test object[19].

The second technique used for probing microscale boundary layers is based on Schlieren photography, which is a method for making visible the locations of gradients in the refractive index of air, caused by gradients in the air temperature. Gates and Benedict (1963) supply a clear explanation and many technical details on the method[19]. They demonstrated that still photographs of Schlieren images provide a means for obtaining quantitative information on the shapes of the "plumes" of air caused by differential heating, either through warming or cooling of the object relative to the surrounding air. Perhaps more important, they showed that motion pictures of Schlieren images provide a means for obtaining quantitative information on the rates of movement of air within the plumes, particulary in the quasi-laminar flow of free convection.

Analysis of motion pictures photographed simultaneously from several directions and of individual frames from those pictures yields data with which to calculate the cross-sectional area of a plume and the rate of flow through that area. Combined with information on the difference in temperature between the plume and the surrounding air — obtained with a thermocouple — one can calculate the rate of flow of heat through the cross-sectional area as a first approximation of the rate of heat transfer between the object and the airstream. This, in turn, can lead to evaluation of the convective heat transfer coefficient, or conductance, of the boundary layer, as discussed in (**9**) of this Box.

Finally, many techniques for estimating values of dynamic parameters in the energy balance involve the use of a "controlled environment chamber" in which essentially all physical, environmental variables — mainly temperatures, wind speeds, humidity, and shortwave radiation — are either controlled or are continually monitored by the investigator. The major simplification produced by such a chamber — a large-animal sized Type B or Type D cuvette, using the terminology of **Box 10-3** — is that, because the walls and the air are at the same temperature, one can say that $T_{OP} = T_a$.

6) Estimation of metabolic rates involved in the energy balance of an animal. The use of a controlled environment chamber for estimating the working metabolic rate consists, in principle, of monitoring the amount of energy that emanates continuously from the animal in excess of the energy involved in the physical environment. When there is essentially no shortwave flux being introduced into the chamber, one may treat it as a Type B closed system and monitor the rate of rise in the temperature of the chamber air as a measure of (**M**) or (M-LE). Alternatively, one may use the chamber as a Type D open system and monitor the rate of cooling required to maintain a constant temperature of circulating chamber air as a measure of (**M**) or (M-LE). Either way, the principle is that of a calorimeter.

As we suggested, while the controlled environment chamber may be used as a calorimeter, it is more often used merely to produce a constant, known thermal environment. In such an environment, a subject can wear a face mask by means of which the rate of "consumption" of oxygen can be monitored. The working metabolic rate is then estimated on the basis that 1 Liter Oxygen min^{-1} = 338 W. (See **Appendix B**).

7) Estimation of the whole-body conductance of an animal, h_b. We mention, in (**6**) just above and in relation to **Eq.(B15-4)**, that by exposing an animal in a calorimeter, measuring its rate of heat production, (**M**), its surface area, (**A**), and its rectal and surface temperatures, ($\mathbf{T_{re}}$) and ($\mathbf{T_s}$), one may calculate an estimate of whole-body conductance, ($\mathbf{h_b}$) or its inverse, (**I**), as $h_b = M/A(T_{re} - T_s)$. Further, one may then obtain an estimate of $k_b = h_b(\Delta z)$ from the reported value of ($\mathbf{h_b}$).

8) Estimation of the coat conductance of an animal, h_f. While the kind of calorimetric method mentioned above is appropriate for a living animal whose whole-body conductance one expects to change as metabolic and environmental conditions change, one may estimate the conductance of a hair coat, ($\mathbf{h_f}$), by means of a calculation based on data from another straightforward method. Heat flow is held in equilibrium between a source and a sink, with a material of unknown conductance between them. For example, if the experimenter covers a metal chamber — customarily of the approximate size and shape of the animal under study — with a close-fitting sample of the animal's hair coat, and he monitors the power, (**Q**), required to maintain a constant temperature, ($\mathbf{T_1}$), within the chamber, he may estimate the coat conductance as $h_f = Q[A(T_1-T_2)]^{-1}$, where ($\mathbf{T_2}$) is the equilibrium temperature on the exterior of the haircoat. Further, one may then obtain an estimate of $k_f = h_f(\Delta z)$ from the estimated value of ($\mathbf{h_f}$) and the measured thickness of the coat.

As we comment in **Note 3** of **Chapter 15**, Campbell *et al.* (1980) used this method, and reported results from others who used it, to estimate the effects of wind speed on ($\mathbf{h_f}$), a problem justifying the effort to construct and use a life-sized simulation of the animal. The effect of wind depends partly on the size and shape of the animal, and thereby on the dimensions of its boundary layer; otherwise the experiment could have been performed with heat flowing from a source to a sink through a simple panel of the hair coat material.

9) Estimation of the whole-body convective transfer coefficient of an animal, h_c. Using a metal casting of a small animal, one may obtain an estimate of ($\mathbf{h_c}$) by the same procedure as in the second method outlined for a leaf in (**10**) of **Box 10-3**. A pre-heated casting of the animal, exposed in a wind tunnel in which the air temperature is held constantly at ($\mathbf{T_a}$), cools at an observed rate. Note that this procedure bears a resemblance to the one described by **Eqs.(B15-5)** above, where ($\mathbf{A_e}$) is estimated by observing the cooling of a casting by radiation in a vacuum; whereas, in this method one estimates ($\mathbf{h_c}$), and the cooling takes place by convection in a wind stream of constant temperature.

Earlier we mentioned a second method for estimating ($\mathbf{h_c}$) in connection with the probing of the microscale boundary layer. After estimating (**H**) by calculating the rate of flow of heat through the cross-sectional area of a thermal plume, one estimates the coefficient as $h_c = H\,[A_e(T_x\text{-}T_a)]^{-1}$.

It is one thing to estimate a whole-body parameter for a small animal or a leaf. It is quite another matter to make such an estimate for a large animal. In principle, a third method for estimating ($\mathbf{h_c}$) consists of evaluating $h_c = H\,[A_e(T_x\text{-}T_a)]^{-1}$ after first estimating (**H**) as a residual of the energy balance equation, in a form such as

$$(a_s\, A'\, S') + (M + \Delta - LE) = H_r(T_x\text{-}T_r) + H_c(T_x\text{-}T_a) + H_g(T_x\text{-}T_g).$$

The energy inflows are on the left and the outflows are on the right side. In equilibrium, when $\Delta = 0$, it is an easy task to obtain reasonable estimates of the shortwave radiant heat load, ($a_sA'S'$); the net metabolic rate, (M-LE); and the losses to longwave exchange and conduction to a substrate, $H_r(T_x\text{-}T_r)$ and $H_g(T_x\text{-}T_g)$. The loss to the substrate is usually negligible if the animal is not lying down. The residual is $H = H_c(T_x\text{-}T_a)$. The principal problem with this method lies in the fact that there are so many factors being estimated — from areas to sweat rates — that the errors tend to compound one another. To apply some general wisdom in this context: if the method of residuals seems too easy to be true, it probably is.

We propose that a *method of differences*, for all its shortcomings, is more reliable for estimating the value of ($\mathbf{h_c}$) for a large animal than a *method of residuals*. That is, when one obtains information on the energy balance of, say, a human being in two sets of circumstances, and then takes a difference, many of the factors in the balance — because they are the same for both sets of circumstances — are eliminated in subtraction and do not need to be estimated. On this point we refer the reader to **Note 2a** of **Appendix D** in **Volume 1**. To illustrate this contention we first describe an experiment reported by Douglas Lee[20], and then we describe how one may use his method as a technique for estimating ($\mathbf{h_c}$) — a use he did not intend.

Lee observed subjects who exercised on a treadmill in a glass enclosure located out-of-doors in the Arizona desert. He carried out the experiment in connection with studies of hyperthermia in military and industrial environments. The subjects were healthy young men in shorts, walking on treadmills for 2 hours, with their metabolic work rate, (**M**), controlled by changes in the speed of the treadmill. Within the enclosure the air temperature, the humidity, and the wind speed were all controlled and held constant for each exposure of each subject. Because of a negligi-

ble contact area, (A_c), and the fact that the inner surfaces of glass were at air temperature, $T_{OP} = T_a$ to a first approximation. Each individual subject — with a constant metabolic work rate, (**M**) — was exposed for 2 hours to one combination of air temperature, humidity, and wind speed. Each combination produced a measured sweat rate, (**SR**), and one value of $T_{OP} = T_a$.

The first half of the experiment with each subject took place with a canvas covering placed over the enclosure, so that $S_d \approx 0$. Under these circumstances, Lee developed statistical relationships for each subject, of the form

$$(SR) = a + b\,(T_{OP}) \qquad \text{(B15-6)}$$

where (a) and (b) are regression coefficients. To illustrate the kind of result Lee obtained, we have plotted the data from **Table 15-2**, Set B, according to **Eq.(B15-6)**, as shown in **Fig. B15-10**. In Lee's experiment, with a single metabolic work rate, (a) and (b) had only one value each for each human subject. In general, however, both (a) and (b) appear to be functions of the metabolic work rate, (**M**), as shown in **Fig. B15-10**.

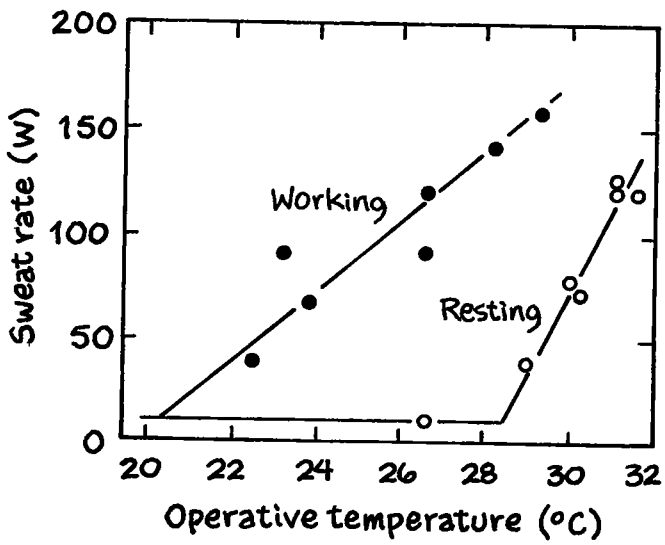

Fig. B15-10 A plot of data from **Table 15-2**, Set B, exhibits the form of relationship in **Eq.(B15-6)** as obtained by Lee in his experiment in Arizona.

Before examining Lee's experiment as a technique for estimating ($\mathbf{h_c}$), we will use our model for the energy balance of a large aninmal to write a mathematical description of the experiment, as follows. With the thermal imbalance as the dependent variable, acting as the surrogate for the sweat rate in our model(I), we write

$$\Delta = \{K_{L^*}\,[(a_s\,A'\,S'/\Sigma H_e) - T_c] + (M - LE)\} + K_{L^*}\,(T_{OP}) \qquad \text{(B15-7a)}$$

(I) **Eqs.(15-5b)** and **(B15-7a)** are the same, but in the first (Δ) is positive when heat is being drawn from the body — hypothermia — whereas in the second (Δ) is positive when heat is being stored in the body — hyperthermia and sweating. The difference is merely a matter of the convenience of interpretation of results, depending upon the problem at hand.

which we note has the same form as Lee's regression relationship in **Eq.(B15-6)** above. Although, in the first half of Lee's experiment, the subjects were observed exercising beneath the canvas cover, so that $S_1' \approx 0$, for now we will keep the analysis general by including it. For the first set of exposures, with the subjects beneath canvas:

$$\Delta_1 = \{K_{L^*}[(a_s A' S_1'/\Sigma H_e) - T_c] + (M - LE)\} + K_{L^*}(T_{OP,1}) \qquad \text{(B15-8a)}$$

For a series of exposures, and with the thermal imbalance acting as the surrogate for the sweat rate, so that $(\Delta_1) = (\mathbf{SR_1})$, we obtain

$$(SR_1) = a_1 + b_1 (T_{OP,1}) \qquad \text{(B15-8b)}$$

in which the shortwave flux density is $(\mathbf{S_1'})$, and the operative temperature is $(\mathbf{T_{OP,1}})$.

In the second half of his experiment with each subject, Lee removed the canvas cover so that the subject was exposed to the Arizona sun. In this case

$$\Delta_2 = \{K_{L^*}[(a_s A' S_2'/\Sigma H_e) - T_c] + (M - LE)\} + K_{L^*}(T_{OP,2}) \qquad \text{(B15-9a)}$$

and

$$(SR_2) = a_2 + b_2 (T_{OP,2}) \qquad \text{(B15-9b)}$$

for a series of values of $(\mathbf{T_{OP,2}})$ with the canvas removed. By placing the same value for (**SR**) in both **Eqs.(B15-8b)** and **(B15-9b)**, Lee obtained a temperature difference

$$(T_{OP,2}) - (T_{OP,1})$$

which he declared to be the temperature equivalent of the shortwave radiant heat load on the subject: a "correction" to $(\mathbf{T_{OP,1}})$ for the addition of the solar radiation. His estimate of the correction, under the conditions of his experiment, was approximately 7.5 °C. We interpret the correction as follows. When the canvas was removed, solar energy replaced some of the energy from heated air in the process of producing the same sweat rate. That is, when (**S'**) increased, $(\mathbf{T_{OP}})$ decreased, since $(\mathbf{T_{OP}})$ does not include information on (**S'**); and $(T_{OP,2}) - (T_{OP,1}) < 0$.

We have simulated Lee's experiment with the mathematical model, and the results are in **Fig. B15-11**. In **Fig. B15-11a** we show the kinds of relationships that Lee must have been sampling with his observations. We exhibit results from four combinations of (**M**) and (**U**), each of which generates a relationship in the form of **Eq.(B15-6)**. Clearly, even with small experimental variations in (**M**) and (**U**) for each subject, Lee would have obtained a very good correlation in his regression model. In fact, he reported values of (**r**) between 0.80 and 0.90.

In **Fig. B15-11b** are values of $(T_{OP,1} - T_{OP,2})$ from our modeling. That difference is a function of (**U**) but is totally independent of (**M**). At lower wind speeds the difference depends more on $(\mathbf{T_{OP}})$ than with stronger winds. In any case, Lee's value of 7.5 to 9 °C for the difference $(T_{OP,1} - T_{OP,2})$ when $U \approx 2$ mps, lies in the middle of our **Fig. B15-11b**, which suggests that our model results are realistic. Our model provides us, in hindsight, with information Lee did not have. For one thing, we must acknowledge the fact that the coefficient (b) in the regression model seems to be a function of (**M**) in **Fig. B15-10** but not in **Fig. B15-11a**. Because we do not have enough information about the experiment that generated the data in **Fig. B15-10**, we will not attempt to address this difference.

The mathematical equivalent of Lee's experiment consists of subtracting **Eq.(B15-8a)** from **Eq.(B15-9a)** under the condition that $\Delta_1 = \Delta_2$. The result of that subtraction is

$$(a_s A' S'/\Sigma H_e)(S_{2'} - S_{1'}) = (T_{OP,1} - T_{OP,2}) \qquad \text{(B15-10a)}$$

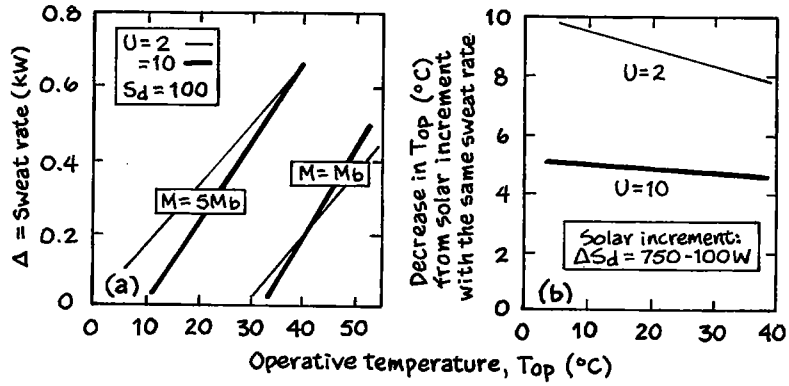

Fig. B15-11 A mathematical simulation reveals the nature of the system Lee was sampling when he monitored the operative temperatures and the sweat rates of exercising individuals within a controlled enclosure in the Arizona desert. **(a)** Relationships of the form of **Eq.(B15-6)**, for four combinations of (**M**) and (**U**). Lee was sampling a system like one of these. **(b)** Removal of a cover from the enclosure resulted in a lower value of ($\mathbf{T_{OP}}$) to produce a given value of (**SR**) compared with the case when the cover was in place. The magnitude of this change is clearly a function of (**U**) but not of (**M**). See the text for discussion.

from which, assuming $H_g = 0$ in the absence of any heat exchange with a substrate,

$$H_c = [(a_s\ A'\ S')(S_{2'} - S_{1'})] / (T_{OP,1} - T_{OP,2}) - H_r \qquad \text{(B15-10b)}$$

In this working equation for the estimation of ($\mathbf{H_c}$), under the controlled condition that $T_{OP} = T_a$, only the parameter (**A'**) needs to be estimated. Granted, (**A'**) is made up of ($\mathbf{A_d}$) and ($\mathbf{A_e}$), for which precise estimates are difficult. But both areas can be estimated well within the precision with which, for example, ($\mathbf{a_s}$) can be measured. The accuracy of the measurement of (**SR**) is not important as long as the condition $\Delta_1 = \Delta_2 = SR_1 = SR_2$ is met. The shortwave flux densities can be measured accurately and precisely, and ($\mathbf{H_r}$) is obtained with a simple calculation. Finally, with an estimate of ($\mathbf{A_e}$) one obtains $h_c = H_c/A_e$.